JEM Journal of Experimental Medicine

ARTICLE

The guanine nucleotide exchange factor Rin-like controls Tfh cell differentiation via CD28 signaling

Lisa Sandner[1], Marlis Alteneder[1], Ramona Rica[1], Barbara Woller[2], Eleonora Sala[3], Tobias Frey[4], Anela Tosevska[5], Ci Zhu[1], Moritz Madern[1], Matarr Khan[1], Pol Hoffmann[1], Alexandra Schebesta[1], Ichiro Taniuchi[6], Michael Bonelli[5], Klaus Schmetterer[4], Matteo Iannacone[3,7], Mirela Kuka[3], Wilfried Ellmeier[1], Shinya Sakaguchi[1], Ruth Herbst[8], and Nicole Boucheron[1]

T follicular helper (Tfh) cells are essential for the development of germinal center B cells and high-affinity antibody-producing B cells in humans and mice. Here, we identify the guanine nucleotide exchange factor (GEF) Rin-like (Rinl) as a negative regulator of Tfh generation. Loss of Rinl leads to an increase of Tfh in aging, upon in vivo immunization and acute LCMV Armstrong infection in mice, and in human CD4⁺ T cell in vitro cultures. Mechanistically, adoptive transfer experiments using WT and Rinl-KO naïve CD4⁺ T cells unraveled T cell–intrinsic GEF-dependent functions of Rinl. Further, Rinl regulates CD28 internalization and signaling, thereby shaping CD4⁺ T cell activation and differentiation. Thus, our results identify the GEF Rinl as a negative regulator of global Tfh differentiation in an immunological context and species-independent manner, and furthermore, connect Rinl with CD28 internalization and signaling pathways in CD4⁺ T cells, demonstrating for the first time the importance of endocytic processes for Tfh differentiation.

Introduction

Small GTPases have been described as regulators of a variety of fundamental processes such as cell proliferation, differentiation, or survival, with Rab GTPases primarily being involved in trafficking processes (Agola et al., 2011; Pfeffer, 2013). They act as so-called molecular switches, binding to either guanosine diphosphate (GDP; inactive state) or guanosine triphosphate (GTP; active state). The change between the two conformational states is carried out by guanine nucleotide exchange factors (GEFs) and GTPase-activating proteins (Simanshu et al., 2017). GEFs facilitate the release of GDP, thereby enabling the binding of GTP to the G protein (Bos et al., 2007). To this date, several families of GEFs for Rab GTPases have been described, with a large group comprising the Vps9 domain–containing family where the Vps9 domain catalyzes the nucleotide exchange (Carney et al., 2006; Hama et al., 1999).

Ras-interaction/interference (Rin) proteins belong to this family and consist of four members called Rin1–3 and Rin-like (Rinl). Rin1–3 functions were elucidated in several in vitro and in vivo studies. They were described as GEFs for Rab5 sharing besides the Vps9 domain, also Src homology 2 (SH2), proline-rich (PR), RIN family homology (RH), and Ras association (RA) domains. The clinical outcome of deficiencies or overexpression in Rin1–3 range from neurological conditions like Alzheimer's disease to macrocephaly, alopecia, cutis laxa, and scoliosis syndrome (Kajiho et al., 2003; Saito et al., 2002; Tall et al., 2001). The latest member of the Rin protein family, Rinl, was originally identified as an interaction partner of the muscle-specific receptor tyrosine kinase MuSK. The structure of Rinl highly resembles the structure of other Rin proteins; however, the RA domain is absent. Previous studies identified Rinl as GEF for Rab5 and Rab22 (Woller et al., 2011) and demonstrated its interaction with ankyrin-repeat and sterile-alpha motif (SAM) domain–containing (Anks) protein Odin, thereby facilitating EphA8 degradation (Kajiho et al., 2012). Interestingly, high Rinl expression was detected in lymphoid organs which indicates a role of Rinl in lymphoid cells. However, knowledge of the function of Rinl in primary cells was missing.

T follicular helper cells (Tfh) are a subset of CD4⁺ T helper (Th) cells and were first described to be present in human tonsils

[1]Division of Immunobiology, Institute of Immunology, Center for Pathophysiology, Infectiology and Immunology, Medical University of Vienna, Vienna, Austria; [2]Center for Brain Research, Medical University of Vienna, Vienna, Austria; [3]School of Medicine, Vita-Salute San Raffaele University and Division of Immunology, Transplantation, and Infectious Diseases, Istituto di Ricovero e Cura a Carettere Scientifico (IRCCS) San Raffaele Scientific Institute, Milan, Italy; [4]Department of Laboratory Medicine, Klinisches Institut für Labormedizin (KILM), Anna Spiegel Research Building, Medical University of Vienna, Vienna, Austria; [5]Internal Medicine III, Division of Rheumatology, Medical University of Vienna, Vienna, Austria; [6]Laboratory for Transcriptional Regulation, RIKEN Center for Integrative Medical Sciences, Kanagawa, Japan; [7]Experimental Imaging Center, Istituto di Ricovero e Cura a Carattere Scientifico (IRCCS), San Raffaele Scientific Institute, Milan, Italy; [8]Institute of Specific Prophylaxis and Tropical Medicine, Center for Pathophysiology, Infectiology and Immunology, Medical University of Vienna, Vienna, Austria.

Correspondence to Nicole Boucheron: nicole.boucheron@meduniwien.ac.at; Ruth Herbst: ruth.herbst@meduniwien.ac.at.

and blood (Kim et al., 2001; Schaerli et al., 2000). They are localized in germinal centers (GCs) and express high levels of CXC chemokine receptor 5 (CXCR5) while having low levels of CC chemokine receptor 7 (CCR7), thus being able to migrate to B cell follicles to provide help for B cells (Kim et al., 2001; Schaerli et al., 2000). Tfh are important players in the immune response against pathogens like bacteria or viruses and were also implicated in diseases including autoimmune diseases, immunodeficiencies, allergic asthma, and lymphomas (Tangye et al., 2013). Moreover, they are important for the generation of high-affinity antibody responses after for example flu vaccines and SARS-CoV-2 infections (Gong et al., 2014; Kaneko et al., 2020). Therefore, identifying factors that control Tfh differentiation and function is pivotal for the development of new treatments, diagnostic tools, and vaccines.

Since the identification of B cell lymphoma (Bcl) 6 as a major transcription factor (TF) of Tfh (Johnston et al., 2009; Nurieva et al., 2009; Yu et al., 2009), substantial progress was made in identifying factors involved in the generation and function of these cells. The differentiation of Tfh was found to be a process in multiple stages facilitated by numerous factors. It was shown that CD28-deficient mice show reduced Th1 and Tfh cell expansion after infection or immunization (Shahinian et al., 1993; Walker et al., 1999). In addition, CD28 was reported to be important for the early stage of Tfh differentiation, while inducible costimulator (ICOS) was identified as a key factor for sustaining Tfh differentiation (Weber et al., 2015).

Here, we used Rinl-deficient mice to study the role of Rinl in vivo. Gene expression studies revealed high *Rinl* abundance in T cells. Further analysis of lymphoid organs and adoptive transfer experiments showed an increase of Tfh in the absence of Rinl upon aging, immunization, and lymphocytic choriomeningitis virus (LCMV) Armstrong infection. This universal regulation of Tfh differentiation under different immunological settings is due to T cell–intrinsic effects and is dependent on the GEF function of Rinl. Transcriptome analysis of naïve CD4$^+$ T cells led to the identification of CD28 as an upstream regulator being affected by loss of Rinl. We show that Rinl plays a role in the regulation of CD28 internalization, which produced qualitative changes in CD28 downstream signaling ex vivo and shaped the differentiation into Tfh after CD28 induction in vivo.

Taken together, our findings suggest Rinl as a novel regulator of Tfh differentiation, highlighting the role of GEFs in Th cell differentiation through involvement in trafficking of signaling receptors and subsequent changes in their signaling strength and/or quality.

Results

Rinl controls the homeostasis of CD4$^+$ Th cells in secondary lymphoid organs

The family of Rin proteins includes four members termed Rin1–3 and Rinl, all sharing the SH2, Vps9, and RH domains. The RA domain is present in Rin1–3 but absent in Rinl, suggesting differences in function and/or localization of this GEF compared with the other family members (Fig. S1 A; Woller et al., 2011). Previously performed tissue expression analyses reported the highest Rinl expression in the murine thymus, spleen, and LN (Yue et al., 2014). Indeed, analysis of *Rinl* expression in WT mice showed the highest abundance of *Rinl* in lymphoid organs such as the thymus, spleen, bone marrow (BM), and LNs (Fig. S1 B; Woller et al., 2011). To dissect the role of Rinl in vivo, Rinl-KO mice were generated by knock-in (KI) of a STOP-internal ribosome entry site (IRES)–LacZ::GFP cassette in the reading frame of exon 4 followed by floxed neomycin. The resulting *Rinl*$^{+/KI\text{-}neo}$ mice were crossed to CMV-Cre mice to delete the neomycin (Fig. S1 C). The insertion led to an inactivation of the *Rinl* allele and the absence of Rinl protein in Rinl$^{KI/KI}$ mice as demonstrated by immunoblot assay, but GFP or β-Gal were not detectable (Fig. S1 D). The inactivated allele is henceforth referred to as a "knockout" allele (Rinl-KO). Rinl-KO mice were developmentally normal and fertile being born at normal Mendelian frequencies. Due to the high expression of *Rinl* in the thymus, we first aimed to study T cell development in WT and Rinl-KO mice. Frequencies of DN, DP, and CD4$^+$/CD8$^+$ SP subsets were comparable between Rinl-deficient and control mice indicating Rinl to be dispensable for the development of T cells (Fig. S1, E and F). As *Rinl* showed high expression in splenic CD4$^+$ and CD8$^+$ T cells (Fig. S1 G) and also an increase in gene expression in CD4$^+$ effector compared to naïve CD4$^+$ T cells (Fig. S1 H), we analyzed lymphocyte homeostasis in the spleen (Fig. S1 I). We detected a significant relative increase in frequencies of B cells and effector CD4$^+$ (CD4$^+$CD44$^+$) T cells in mice aged between 8 and 12 wk. Furthermore, Rinl-KO mice showed a strong increase in total splenocytes with consequent significantly increased absolute numbers of B and T lymphocytes, in particular effector CD4$^+$ (CD4$^+$CD44$^+$) T cells, whereas CD8$^+$ T lymphocytes were unaltered (Fig. S1, I and J).

Strikingly, aged Rinl-KO mice (36–40 wk) showed splenomegaly, increased spleen weight, and increased splenocyte numbers (Fig. 1, A and B). They accumulated more T cells, CD4$^+$, and effector CD4$^+$ T cells (CD62L$^-$CD44$^+$) compared with WT mice. Additionally, an increase of total Tfh and GC B cells was detected (Fig. 1 C, for gating strategy please refer to Fig. S2 A), while other Th subsets were not altered (Fig. S2, B and C). In LNs of aged mice, an increase in CD4$^+$ and Tfh cell frequencies was also observed in the absence of Rinl (Fig. S2 D) indicating organ-dependent alterations in lymphocyte subsets. Altogether, our immunophenotyping of Rinl mice suggests a regulatory role of Rinl in CD4$^+$ Th cell activation/differentiation, in particular toward Tfh.

Rinl regulates Tfh differentiation and GC B cell generation in homeostasis and upon immunization

To define the role of Rinl in CD4$^+$ Th cells in more detail, we first investigated the differentiation potential of WT and Rinl-KO naïve CD4$^+$ T cells into Th1, Th2, Th17, and regulatory T (Treg) cells in vitro. Frequencies of key cytokine-producing or lineage-specific TF expressing cells of all major Th subsets were comparable suggesting Rinl to be dispensable for regulating differentiation of those Th subsets in vitro (Fig. S3, A and B). First, analyses of Tfh (defined by CXCR5 and PD-1) and GC B cells (defined by GL7 and CD95) were performed in Peyer's patches (PP), a lymphoid structure favoring the generation of those cells due to constant

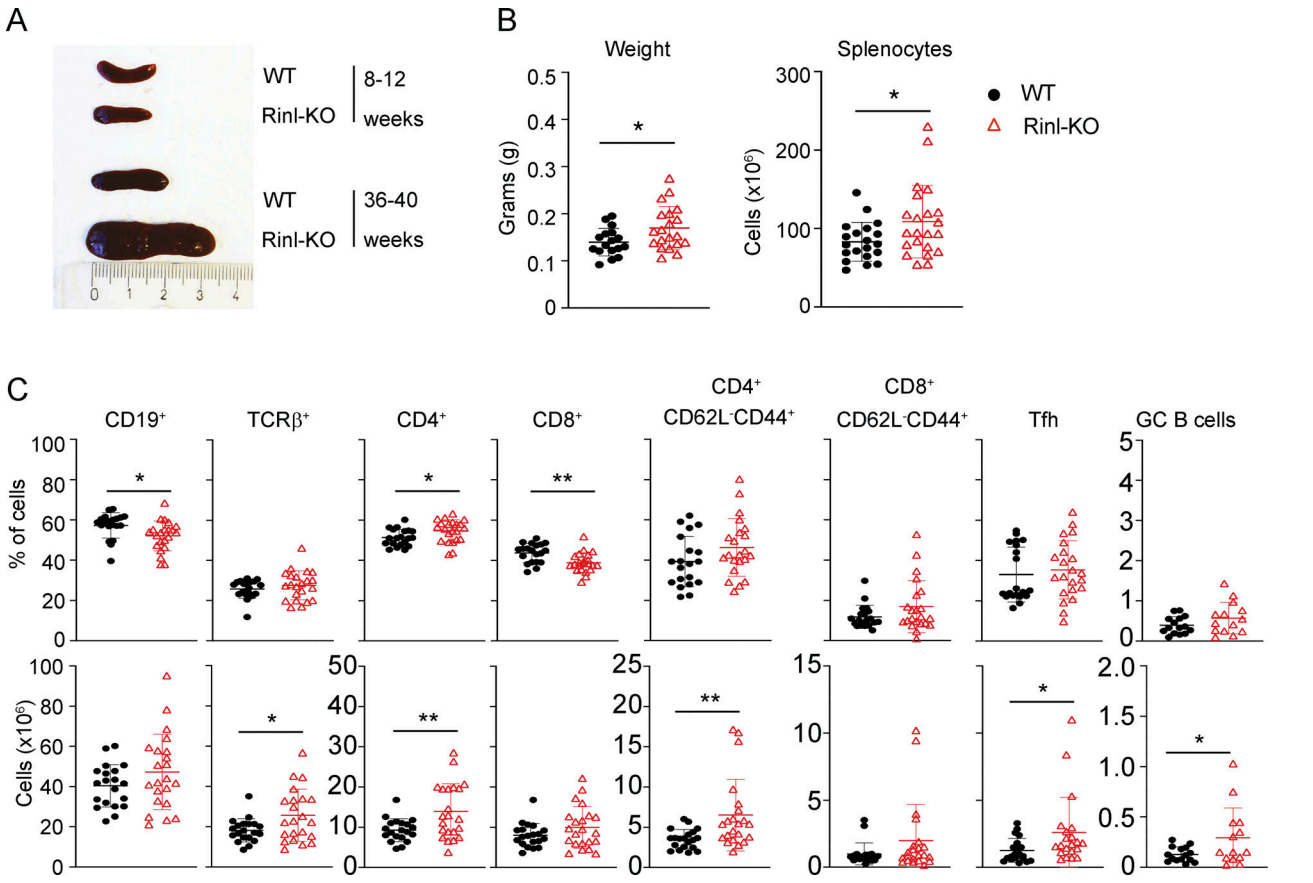

Figure 1. **Absence of Rinl leads to alterations in immune homeostasis in older mice. (A)** Representative picture of spleens of WT and Rinl-KO mice of 8–12 and 36–40 wk of age. **(B)** Diagrams show the weight and total leukocyte count of splenocytes of 36–40 wk old WT and Rinl-KO mice. **(C)** Summary graphs show the percentages (upper panel) and cell counts (lower panel) of major lymphocyte subsets analyzed. The summary of 17–20 mice per genotype analyzed in four independent experiments is shown. Mean ± SEM are shown along individual data points in the graphs. Data were statistically analyzed using unpaired two-tailed *t* tests (B and C). *P < 0.05, **P < 0.01.

stimulation by external factors like the microbiome (Jones et al., 2016). In PPs, Rinl-KO mice showed a significant increase of both cell subsets under homeostatic conditions (Fig. 2, A and B). We furthermore demonstrated a high expression of *Rinl* in Tfh while expression in GC B cells was low (Fig. 2 C), suggesting a specific role of Rinl in the generation of Tfh.

Next, we sought to determine the importance of Rinl during Tfh differentiation following immunization. We immunized WT and Rinl-KO mice intraperitoneally (i.p.) with 100 µg/ml 4-hydroxy-3-nitrophenylacetyl hapten conjugated to ovalbumin (NP-OVA) in the Th2-driving Imject Alum Adjuvant (Alum; Fig. 2 D). As expected, immunization with NP-OVA/Alum led to an increase in Tfh frequencies and cell numbers compared with non-immunized control mice 7 d after immunization. Strikingly, we detected an increase in Tfh in relative and absolute numbers in Rinl-KO mice compared with WT mice (Fig. 2 E) along with an increase in GC B cells. Immunization was also performed using complete Freund's adjuvant (CFA; Fig. S3 C), which augments mostly Th1- and Th17-mediated responses (Ciraci et al., 2016; Yang and Hayglass, 1993). Similar to results gained with Alum, Tfh were significantly increased in Rinl-KO mice in comparison with WT counterparts (Fig. S3 D), whereas other Th subsets were unaltered (Fig. S3 E). To conclude, our data show evidence that Rinl specifically controls the differentiation of Tfh in vivo.

Rinl is a negative regulator of Tfh differentiation upon LCMV infection

We next aimed to study the effect of Rinl on Tfh differentiation in the context of an infection setting. We used an acute infection model with LCMV which induces the generation of virus-specific Th1 and Tfh cells, in addition to a CD8⁺ T cell response (Hale et al., 2013; Marshall et al., 2011; Xu et al., 2015). At day 8 after LCMV infection, Rinl-KO mice showed no change in frequencies of lymphocyte subsets (Fig. 3 A, for gating strategy please refer to Fig. S4, A and B). However, a significant increase in splenocyte numbers was observed, along with a prominent expansion of total CD4⁺ Th cells in Rinl-KO compared with WT mice (Fig. 3 B). Among CD4⁺ T cells, a significant increase of effector CD4⁺ (CD4⁺CD44⁺) and Tfh (PD-1⁺CXCR5⁺) was observed in the absence of Rinl. Moreover, while a similar amount of virus-specific gp66 tetramer–positive CD4⁺ T cells in Rinl-KO and control mice was detected, a higher number of gp66 tetramer–positive PD-1⁺CXCR5⁺ Tfh were present in Rinl-KO mice (Fig. 3 B). The number of gp66 tetramer–positive

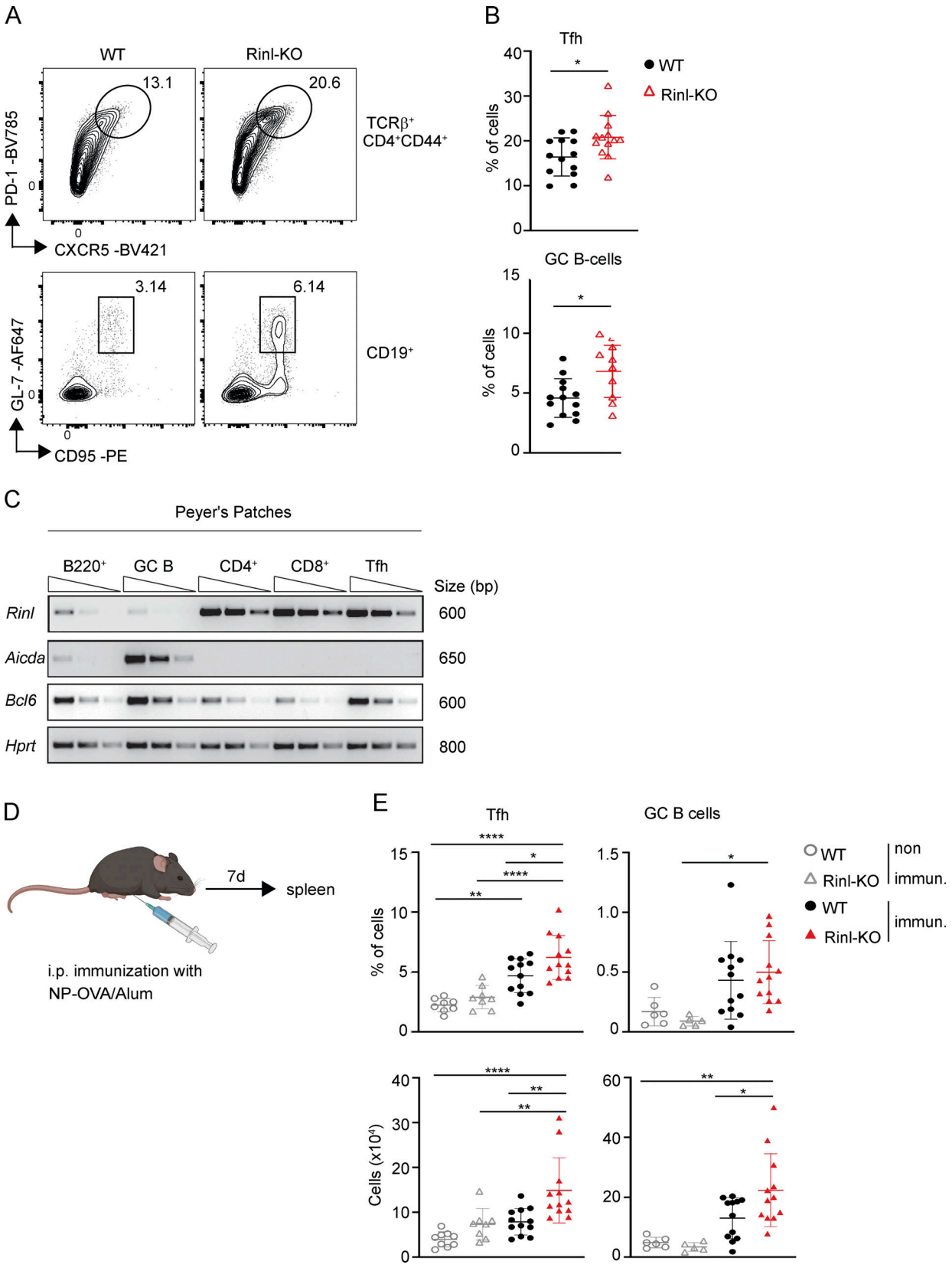

Figure 2. **Rinl controls Tfh and GC B cell generation in homeostasis and upon immunization. (A)** Representative contour plots show Tfh and GC B cells in PP of WT or Rinl-KO mice. Numbers in plots indicate percentages of cells. **(B)** Quantification of A. **(C)** Semi-quantitative PCR of *Rinl*, *Aid*, and *Bcl6* expression in different cell subsets in PP of WT mice. *Hprt* expression was used as control. **(D)** Experimental scheme of immunization experiment. **(E)** Summary graphs depict percentages (upper panel) and cell numbers (lower panel) of Tfh and GC B cells recovered from spleens from non-immunized and immunized WT and Rinl-KO

mice. Data show a summary of 11–13 (B) and 5–8 (E) mice per group analyzed in three to four independent experiments (B and E). Mean ± SEM are shown along individual data points in the graphs. Data were statistically analyzed using unpaired two-tailed *t* tests (B) or one-way ANOVA analysis followed by Tukey's multiple-comparisons test (E). *P < 0.05, **P < 0.01, and ****P < 0.0001. Source data are available for this figure: SourceData F2.

PSGL1$^+$Ly6C$^+$ Th1 was unaltered, indicating a suppressive role of Rinl selectively on Tfh differentiation during viral infection (Fig. 3 B). Similar to immunization experiments, LCMV infection led to an increase in B cells 8 d post infection (dpi) and a significant enhancement of GC B cells and IgG1$^+$ B cells in the absence of Rinl at 21 dpi (Fig. 3, C and D; and Fig. S4 C). Additionally, IgG1 antibody levels, in contrast to IgG2c levels, in the sera of Rinl-KO mice 21 dpi showed a tendency to be elevated in comparison with sera from WT mice (Fig. 3 E). Overall, infection experiments disclosed a role of Rinl in virus-specific Tfh differentiation and generation of virus-specific antibodies.

Rinl has a T cell–intrinsic effect on early Tfh commitment without affecting overall CD4$^+$ T cell survival, activation, proliferation, and migration/localization

To examine the intrinsic role of Rinl in early T cell activation and proliferation in vivo, we crossed WT and Rinl-KO mice with OVA TCR transgenic mice, further named as either WT OT-II$^+$ or Rinl-KO OT-II$^+$ mice. We subsequently performed adoptive transfer experiments in which we isolated WT or Rinl-KO OT-II$^+$ naïve CD4$^+$ CD45.2$^+$ T cells, labeled them with CFSE, and injected them i.v. into CD45.1$^+$CD45.2$^+$ recipient mice (Fig. 4 A). 2 d after immunization, transferred (CD45.2$^+$CD45.1$^-$) CD4$^+$ T cells in draining (popliteal) LNs (dLN) and non-draining (axillary) LNs (ndLN) were analyzed for proliferation, early activation marker expression, and viability (Fig. 4, B–E). We did not observe differences in frequencies of transferred cells, proliferation (defined as CFSE^{low}), activation measured via CD25 and CD69 expression, or viability (Fig. 4, B–E). However, Rinl-KO OT-II$^+$ cells showed a significantly higher frequency of CD44$^+$ effector and CXCR5$^+$/ICOS$^+$ Tfh cells (Fig. 4, F and G; Choi et al., 2011). We furthermore performed immunohistochemistry of dLNs at day 3 and 5 after immunization to define the localization of transferred WT or Rinl-KO CD4$^+$CD45.2$^+$ T cells. On day 3 after immunization, we detected antigen-specific CD45.2$^+$ T cells of both genotypes in the T cell area close to the T–B cell border (Fig. 4 H). Further detection of the T cells into the B cell follicles at day 5 suggested proper migration and localization of T cells also in the absence of Rinl during early activation (Fig. 4 H). To conclude, our data demonstrate a role for Rinl in early commitment toward effector cells and especially Tfh but not in overall T cell activation, proliferation, survival, and migration.

Rinl has a T cell–intrinsic effect on GC Tfh differentiation without affecting T cell homing

To study the differentiation potential of WT or Rinl-KO OT-II$^+$ CD4$^+$ T cells into full GC Tfh, we injected WT or Rinl-KO OT-II$^+$ naïve CD4$^+$CD45.2$^+$ T cells into CD45.1$^+$ recipient mice and performed footpad (FP) immunization with NP-OVA/Alum the next day (Fig. 5 A). Strikingly, on day 7 after immunization, we detected a significant enhancement of PD-1$^+$CXCR5$^+$ Tfh among Rinl-KO OT-II$^+$ T cells compared with WT OT-II$^+$ T cells, indicating a T cell–intrinsic regulation of GC Tfh commitment upon loss of Rinl (Fig. 5, B and C). We assessed migration of T cells in dLNs, spleens, and ndLNs. Both WT and Rinl-KO transferred (CD45.2$^+$CD45.1$^-$) CD4$^+$ T cells were almost exclusively found in dLNs. Furthermore, frequencies in dLNs were unaltered between WT and Rinl-KO OT-II$^+$ T cells, indicating no impact of Rinl on the homing capacity of cells to secondary lymphoid organs (Fig. 5 C). The expression of the Tfh master TF Bcl6 was not increased in the absence of Rinl in PD-1$^+$CXCR5$^+$ Tfh cells; however more CXCR5$^+$Bcl6$^+$ cells were detected in Rinl-KO transferred cells compared with WT cells (Fig. 5 D), indicating that more naïve CD4$^+$ T cells were fated to become Tfh cells in absence of Rinl without affecting however Bcl6 levels. ICOS$^+$ cell frequencies and ICOS expression were significantly higher among transferred Rinl-KO effector (CD44$^+$) CD4$^+$ T cells (Fig. S5 A) and CXCR5$^+$PD-1$^+$ Tfh compared with the WT counterparts (Fig. 5 E), showing that Rinl regulates pathways that control ICOS levels. Given the essential role of IL-21 in the generation of Tfh cells (Vogelzang et al., 2008), we assessed IL-21 production by effector CD4$^+$ T cells and Tfh. IL-21 production was similar in WT cells and cells lacking Rinl (Fig. S5 B and Fig. 5 F). As Tfh were described as high IL-2–producing cells (DiToro et al., 2018), we also determined their IL-2 production and observed higher IL-2 production and IL-2$^+$ frequencies of effector and Tfh cells lacking Rinl in contrast to the WT counterparts (Fig. S5 C and Fig. 5 G). By performing immunohistochemistry of dLNs, we further evaluated that both WT and Rinl-KO T cells are capable of residing within the B cell follicles and started to form clusters (Fig. 5 H). Taken together, our data indicate that Rinl regulates full GC Tfh differentiation in a T cell–intrinsic way via pathways that affect ICOS surface levels and IL-2 production, without affecting Bcl6 or IL-21 expression as well as migration of Tfh cells to GCs.

The regulation of Tfh differentiation by Rinl does not involve trans-effects or additional T cell–extrinsic functions

Next, we investigated possible trans-effects due to soluble mediators released by CD4$^+$ T cells by co-transferring WT OT-II$^+$ naïve CD4$^+$CD45.1$^+$ T cells and either WT or Rinl-KO OT-II$^+$ naïve CD4$^+$CD45.2$^+$ T cells i.v. into TCR$\alpha^{-/-}$ mice (Fig. 6 A). The same frequencies of TCRβ^+ cells and Tfh were detected in mice co-transferred with WT OT-II$^+$CD45.1$^+$/WT OT-II$^+$CD45.2$^+$ and WT CD45.1$^+$/Rinl-KO CD45.2$^+$ T cells 7 days after immunization (Fig. 6, B and C). Among Tfh cells, Rinl-KO CD45.2$^+$ cells were significantly increased compared with WT CD45.2$^+$ cells co-transferred with WT CD45.1$^+$ cells, showing an enhanced T cell–intrinsic Tfh differentiation potential of Rinl-deficient CD45.2$^+$ cells. In contrast, no difference in CD45.1 and CD45.2 proportion was detected in the non-Tfh (PD-1$^-$CXCR5$^-$) population, suggesting no influence of soluble factors of Rinl-KO T cells on WT T cells favoring Tfh differentiation (Fig. 6, B and C).

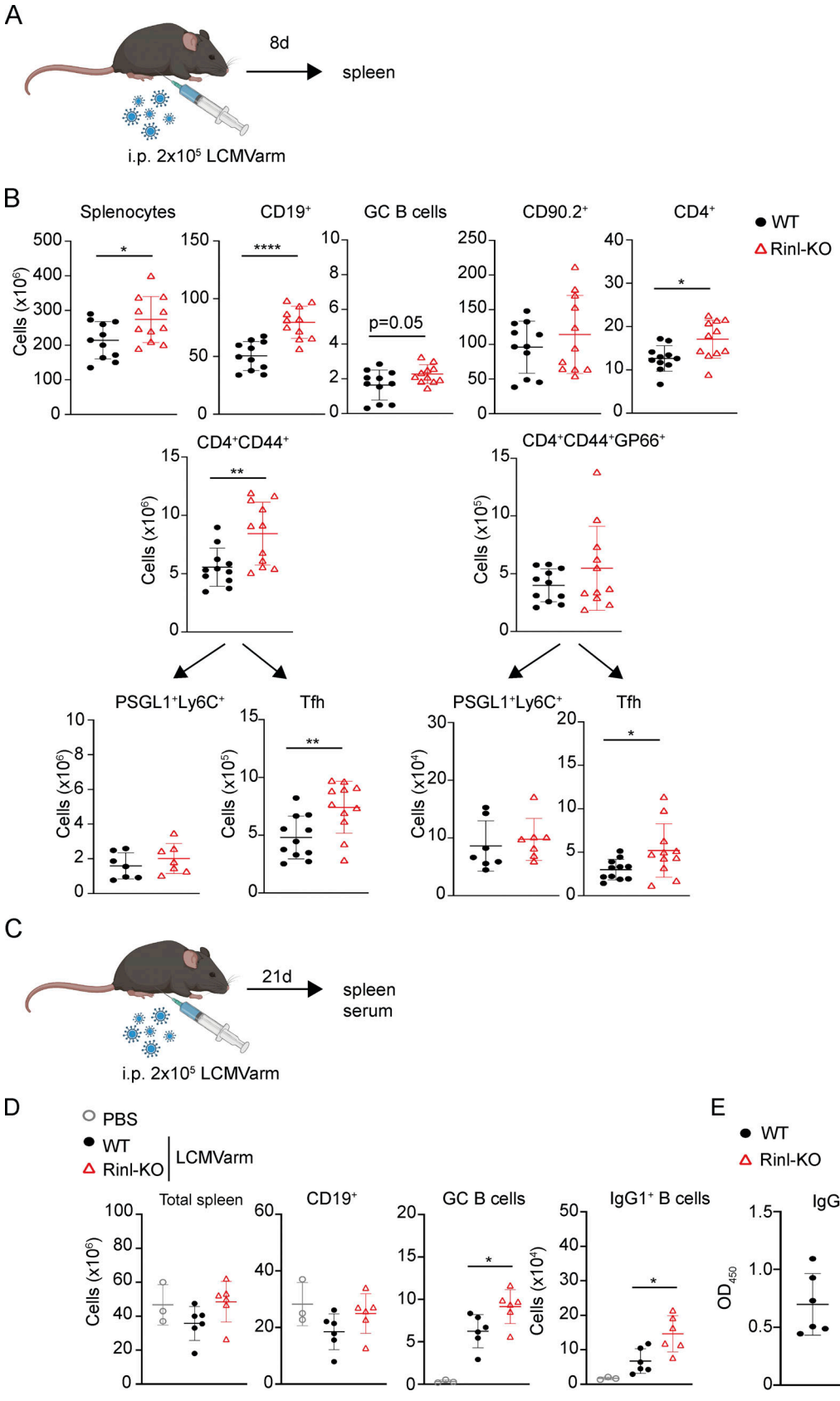

Figure 3. **Rinl regulates Tfh and B cell response upon LCMV Armstrong infection. (A)** Experimental scheme. **(B)** Summary diagrams depict cell numbers of a variety of lymphocyte subsets from spleens of WT and Rinl-KO mice 8 dpi. **(C)** Experimental scheme of LCMV Armstrong infection to study B cell responses. **(D)** Summary diagrams depict cell numbers of B cell subsets from spleens of WT and Rinl-KO mice 21 dpi. **(E)** Virus-specific IgG1 and IgG2c levels in serum 21 dpi. Data show a summary of 11 (B) or 6 (D and E) mice per group analyzed in three (B) or two (D and E) independent experiments. Mean ± SEM are shown along individual data points in the graphs. Data were statistically analyzed using unpaired two-tailed *t* tests. *P < 0.05, **P < 0.01, ****P < 0.0001.

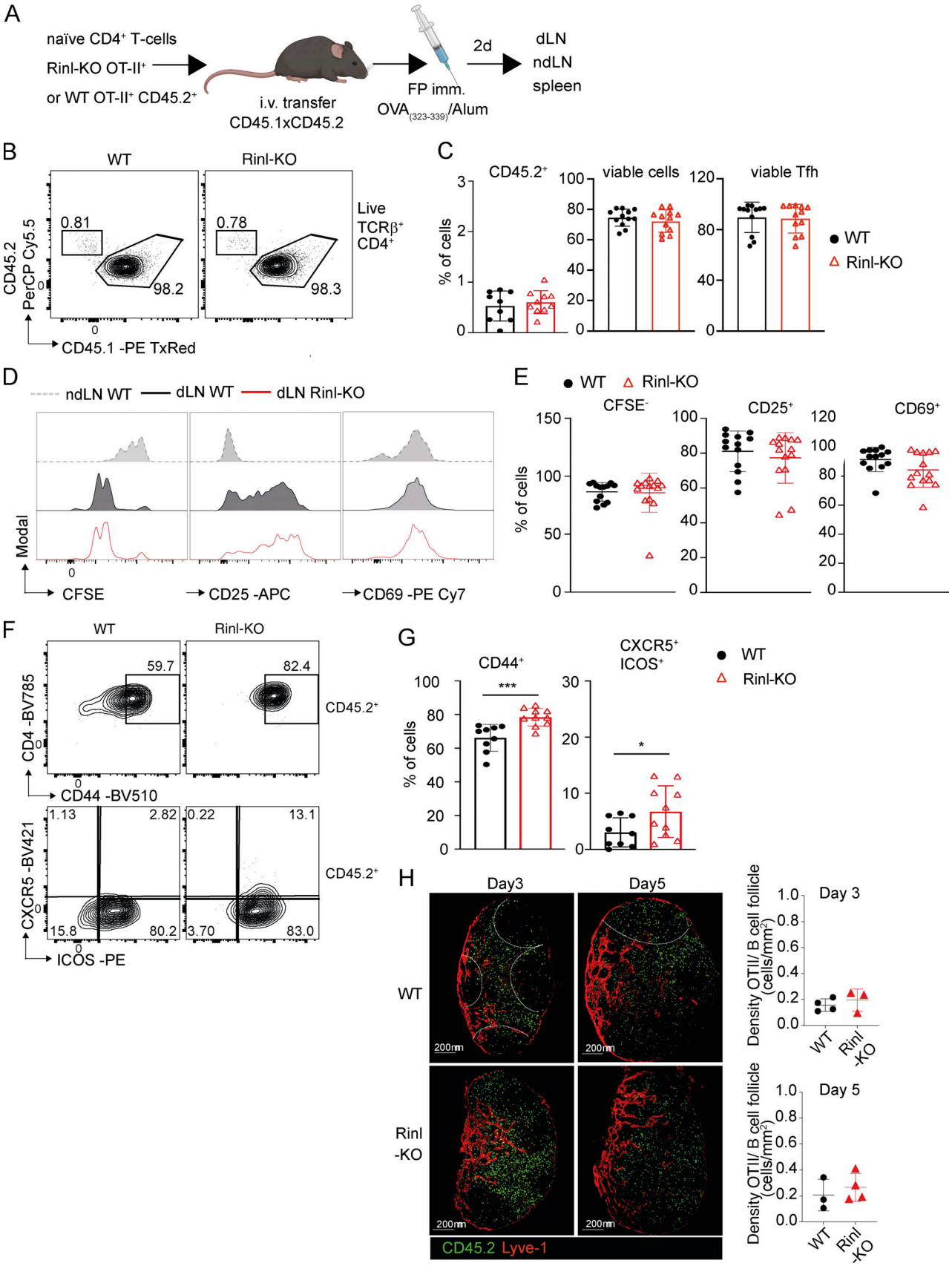

Figure 4. **Early Tfh commitment in Rinl-KO mice is T cell intrinsic. (A)** Experimental scheme. **(B)** Representative contour plots of dLN samples taken from WT and Rinl-KO mice showing transferred cells (CD45.2+). **(C)** Summary of B (left panel), total viable transferred cells assessed using viability dye (middle

panel), and viable Tfh (right panel). **(D)** Representative histograms of proliferation (CFSE) and CD25 and CD69 expression on transferred (CD45.2⁺CD45.1⁻) CD4⁺ T cells. **(E)** Summary of A. **(F)** Representative contour plots of dLN samples taken from WT and Rinl-KO mice showing effector cells (CD44⁺) and pre-Tfh (ICOS⁺CXCR5⁺). **(G)** Summary of F. **(H)** Representative confocal images of dLNs on days 3 and 5 after immunization. Dashed lines represent the edges of B cell follicles and were set based on B220 staining. Ag-specific CD45.2⁺ cells are shown in green, and Lyve-1 staining in red. Images are representative of at least three to five LNs from two independent experiments. Quantifications are shown alongside. Data show a summary of 9–10 (C and G) and 13–14 (E) mice per group analyzed in two (C and G) or three (E) independent experiments. Mean ± SEM are shown along individual data points in the graphs. Data were statistically analyzed using unpaired two-tailed *t* tests. *P < 0.05, ***P < 0.001.

To exclude the involvement of non-T cells like DCs or B cells in Tfh differentiation in the absence of Rinl, we crossed Rinl-KO mice to TCRα KO mice which lack all αβT cells further named Rinl-KO TCRα-KO mice. We then performed adoptive transfer experiments of WT OT-II⁺ naïve CD4⁺ T cells into either TCRα-KO or Rinl-KO TCRα-KO mice (Fig. 6 D). 7 d after immunization, comparable frequencies and cell counts of T cells and Tfh were detected in both recipient mice, indicating no significant effect of Rinl-KO non-T cells on Tfh differentiation (Fig. 6 E).

Collectively, adoptive transfer experiments indicate a T cell–intrinsic regulation of Tfh differentiation by Rinl, which is not the consequence of an increase in secreted factors. This is also not due to changes in T cell homing or follicle formation but is the result of enhanced commitment toward this Th subset in the absence of Rinl. In addition, our data strongly suggest that other immune cells are not contributing to the enhanced Tfh differentiation when Rinl is not present.

Rinl is a regulator of CD28 signaling pathway

To elucidate the molecular mechanisms by which Rinl regulates Tfh differentiation, we performed a transcriptome analysis of ex vivo sorted naïve CD4⁺ T cells (CD4⁺CD62L⁺CD44⁻) from spleens of WT and Rinl-KO mice using RNA sequencing (RNA-seq) approaches. Globally, 123 genes were downregulated and 217 genes upregulated in Rinl-KO naïve CD4⁺ T cells compared with WT cells (Fig. 7 A). Importantly, Ingenuity Pathway Analysis identified STAT3 and CD28 as the most dysregulated upstream regulators (Fig. 7 B). STAT3-regulated genes were mostly related to type I IFN signaling (Table 1), implying a role of Rinl in this pathway. Given the function of Rinl as GEF for Rab5 GTPases, and therefore its involvement in receptor endocytosis, we focused our study on CD28, an early co-stimulation receptor with strong implications for T cell differentiation, ICOS surface levels, and robust IL-2 secretion (McAdam et al., 2000; Thompson et al., 1989). Moreover, CD28 was previously demonstrated to be indispensable for Tfh and GC formation (Ferguson et al., 1996; Weber et al., 2015), and fine-tuning of CD28 signaling as well as CD28 signaling strength were described as crucial factors in Tfh differentiation (Wan et al., 2021; Wang et al., 2015).

To study this in more detail, we first analyzed CD28 expressions on naïve and effector CD4⁺ T cells, which were comparable between WT and Rinl-KO conditions (Fig. 7 C). CD28 expression is regulated by constant turnover of the receptor (Badour et al., 2007; Céfaï et al., 1998). As Rinl is a GEF for Rab5 GTPases involved in receptor trafficking, we examined its role in CD28 endocytosis and downstream signaling such as phosphorylation of SLP76, Akt, or Erk1/2. Interestingly, endocytosis assays showed that the internalization of CD28 was significantly decreased in Rinl-KO effector CD4⁺ T cells (CD4⁺CD44⁺) with a tendency to being reduced also in naïve CD4⁺ T cells (CD4⁺CD44⁻; Fig. 7 D). Moreover, combined αCD3ε and αCD28 stimulation of CD4⁺ T cells led to strongly reduced pSLP76 (Ser376), which was described to negatively regulate T cell activation (Di Bartolo et al., 2007) with unchanged early Akt and Erk1/2 phosphorylation (Fig. 7 E). Intriguingly, after the stimulation of cells with TCR and CD28 but not with TCR alone, in culture for 48 h, we detected reduced levels of Erk1/2 phosphorylation in Rinl-KO cells (Fig. 7, F and G). The Erk pathway was recently described as a repressive factor of Tfh differentiation and its sequential requirement during this process has been highlighted (Wan et al., 2021). In addition, ICOS expression was significantly stronger induced in the absence of Rinl only in the presence of CD28 co-stimulation (Fig. 7, H and I). These data together suggest an effect of Rinl in shaping CD28 signaling quality.

To test whether CD28 signaling strength has an effect in the absence of Rinl, we cultured naïve CD4⁺ T cells with constant αCD3ε and low and high αCD28 concentrations for 3 d and assessed proliferation and IL-2 production (Fig. 8, A–C). Interestingly, we detected a significant increase in proliferation and IL-2 production in Rinl-KO cells stimulated with lower αCD28 concentration compared with WT cells (Fig. 8, B and C). Proliferation in Rinl-KO T cells was also enhanced in a more physiological model when activation was performed with BM-derived dendritic cells (BMDCs) in the presence of CTL4-Ig (Fig. 8 D). Collectively, these data suggest a role of Rinl in fine-tuning CD28 downstream events, which mediate early Tfh commitment.

Rinl is a regulator of CD28 signaling in vivo

We next aimed to study the effect of Rinl on CD28 signaling and subsequent Tfh differentiation in vivo. Therefore, we treated WT or Rinl-KO mice with αCD28 or isotype control 1 d before i.p. immunization with NP-OVA Alum. Tfh cell frequency was analyzed on day 7 after immunization (Fig. 9 A). In agreement with a published study (Vogelzang et al., 2008), CD28 induction led to an increase in Tfh differentiation in both genotypes. Importantly, αCD28 treatment led to similar frequencies of Tfh between the genotypes in contrast to isotype treatment where we detected an increased differentiation into Tfh in spleens of Rinl-KO mice (Fig. 9, B and C). Of note, Tfr (FoxP3⁺ Tfh) frequencies were not affected by αCD28 treatment (Fig. S5 D). To understand whether disruption of signaling events subsequent to CD28 co-stimulation affects Tfh differentiation in the absence of Rinl, we inhibited ICOS signaling in vivo by injection of ICOSL-blocking antibodies during adoptive transfer and after immunization (Fig. 9 D). As previously shown (Weber et al., 2015), ICOSL blocking strongly inhibited Tfh differentiation, however almost

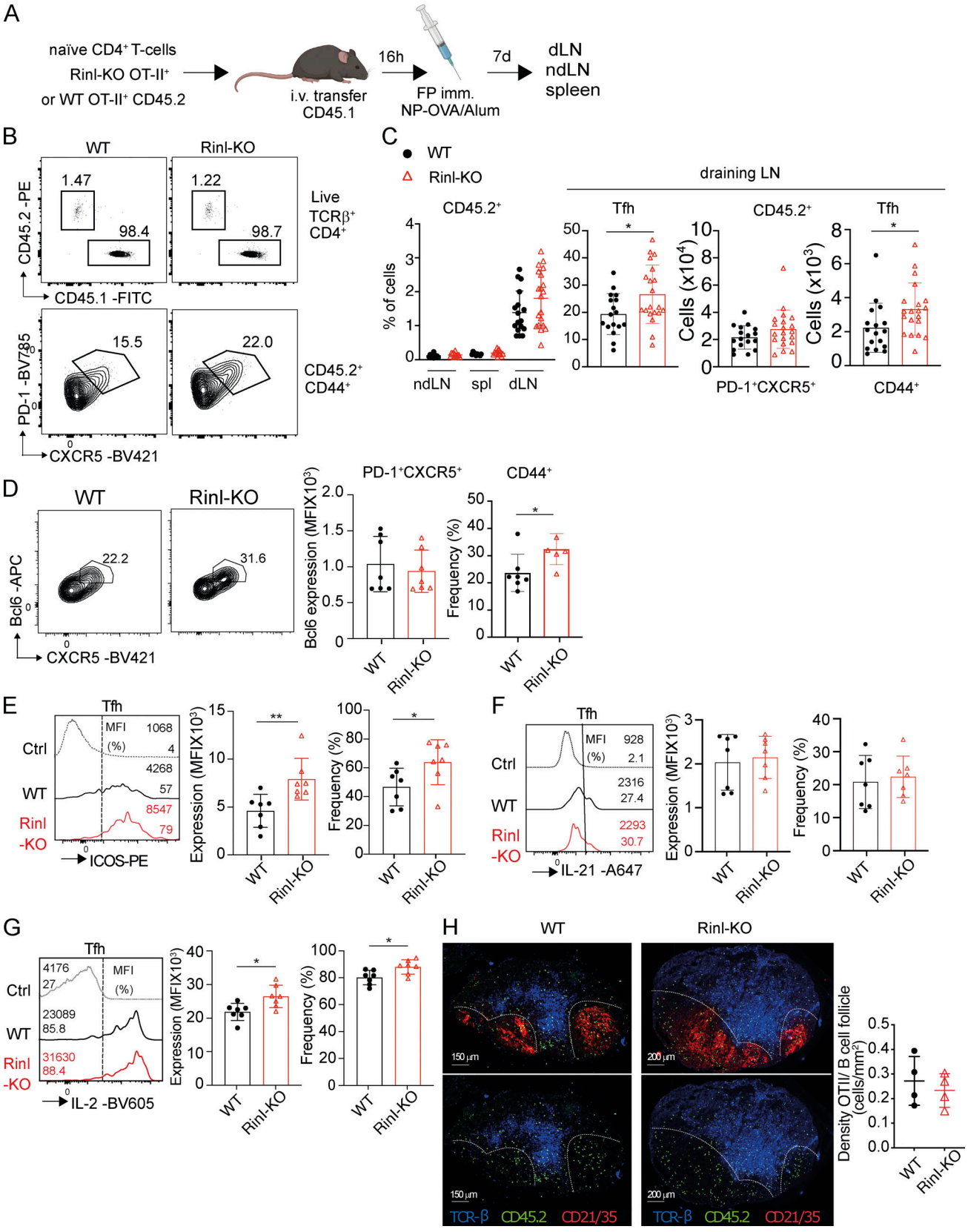

Figure 5. **Increased GC Tfh differentiation in Rinl-KO mice is T cell intrinsic. (A)** Experimental scheme. **(B)** Representative contour plots of dLN samples taken from WT and Rinl-KO mice showing transferred cells (CD45.2$^+$) and Tfh (PD-1$^+$CXCR5$^+$). **(C)** Summary of B. **(D)** Representative contour plots of dLN samples taken from WT and Rinl-KO mice showing Tfh (Bcl6$^+$CXCR5$^+$). Diagrams alongside depict Bcl6 expression in Tfh cells defined as PD-1$^+$CXCR5$^+$ (left diagram) and frequencies of Bcl6$^+$CXCR5$^+$ Tfh cells (right diagram). **(E)** Representative histograms of ICOS expression in PD-1$^+$CXCR5$^+$ Tfh. A summary of ICOS

expression (left diagram) and frequencies of ICOS⁺ cells among PD-1⁺CXCR5⁺ Tfh (right diagram) is shown alongside. **(F)** Representative histograms of IL-21 production in PD-1⁺CXCR5⁺ Tfh. A summary of IL-21 expression (left diagram) and frequencies of IL-21⁺ cells among PD-1⁺CXCR5⁺ Tfh (right diagram) is shown alongside. **(G)** Representative histograms of IL-2 production in PD-1⁺CXCR5⁺ Tfh. A summary of IL-2 expression (left diagram) and frequencies of IL-2⁺ cells among PD-1⁺CXCR5⁺ Tfh (right diagram) is shown below. **(H)** Representative confocal images of dLN were collected 7 d after immunization. Dashed lines represent the edges of B cell follicles and were set based on CD21/35 staining (shown in the upper images). TCRβ⁺ cells are shown in blue, Ag-specific CD45.2⁺ cells in green, and CD21/35 in red. Images are representative of at least three to five LNs from two independent experiments. A summary is shown alongside. Data show a summary of 17–20 (C) and 7 (D–G) mice per group analyzed in four (C) and two (D–G) independent experiments. Mean ± SEM are shown along individual data points in the graphs. Data were statistically analyzed using unpaired two-tailed *t* tests. *P < 0.05, **P < 0.01.

to the same extent between WT and Rinl-KO T cells (Fig. 9, E and F). Strong CD28 signaling resulted in comparable Tfh in WT and Rinl-KO mice, and ICOS blocking revealed a similar requirement for ICOS signaling in the absence or presence of Rinl. Altogether, this suggests that Rinl is a negative regulator of Tfh by dampening the effect of CD28 stimulation on CD4⁺ T cells.

The GEF activity of Rinl is required to restrain Tfh differentiation

To mechanistically investigate whether the GEF function of Rinl is required to restrain Tfh differentiation, we generated retroviral constructs carrying either full-length Rinl (mycRinl) or GEF-deficient Rinl (mycRinl-ΔVps9; Deininger et al., 2008; Woller et al., 2011). Both Rinl proteins were tagged with myc. We retrovirally expressed mycRinl and mycRinl-ΔVps9 in preactivated naïve Rinl-KO OTII⁺ CD4⁺ T cells and transferred the cells into congenic hosts 24 h after transduction (Fig. 9 G). As controls, WT and Rinl-KO naïve OTII⁺ CD4⁺ T cells were preactivated and treated as transduced cells and transferred into congenic mice. The mice were immunized into the FP 24 h after transfer of the T cells, and Tfh differentiation was assessed 7 d later in the dLN. Expression of mycRinl and mycRinl-ΔVps9 in transduced cells was assessed by immunoblotting 48 h after transduction (Fig. 9 H). Tfh frequency was enhanced in Rinl-KO conditions, showing that preactivation did not affect the regulatory function of Rinl on Tfh differentiation (Fig. 9, I and J). Importantly, Tfh differentiation was increased in T cells that expressed mycRinl-ΔVps9 in contrast to those that expressed mycRinl, showing that the GEF function of Rinl is required to restrain Tfh differentiation (Fig. 9, I and J).

Human Tfh differentiation is affected by Rinl

As high Rinl expression was also detected in human lymphoid tissues, we next aimed to study its role in human Tfh (Fagerberg et al., 2014). In contrast to murine cells, an in vitro differentiation protocol for human Tfh has been established (Locci et al., 2016). We isolated CD4⁺ T cells from the human peripheral blood of healthy individuals and performed CRISPR-Cas9 knockout of Rinl or control guide RNA. After a successful knockout, we cultured cells under Tfh-skewing conditions. In accordance with the data from the murine experiments, Rinl-KO cells showed a higher differentiation potential into Tfh in vitro suggesting Rinl a negative regulator of Tfh differentiation also in humans (Fig. 10, A and B). To understand whether CD28 is important for the regulation of Tfh differentiation of human T cells in general and also in particular via Rinl, we performed the Tfh differentiation of human naïve CD4⁺ T cells in the absence or presence of CD28 (Fig. 10, C and D). As previously shown for murine T cells (Weber et al., 2015), CD28 was essential for Tfh differentiation of human naïve CD4⁺ T cells. In contrast to non-Tfh skewing conditions, CD28 was essential for proper T cell blast formation and Tfh differentiation in Tfh skewing conditions as shown by the reduced cell size and frequency of CXCR5⁺ cells (Fig. 10, C and D). In the absence of Rinl, blast cell formation or frequency of CXCR5⁺ cells was not altered when CD28 stimulation was missing; however, CXCR5⁺ cells were increased in frequency in the presence of CD28 stimulation (Fig. 10, E and F). These data together strengthen our hypothesis that Rinl regulates Tfh differentiation in humans and mice via a CD28-dependent mechanism.

To further investigate a potential link between Rinl expression, Tfh differentiation, and autoimmunity, we determined the expression levels of Rinl in previously published bulk RNA-seq data from T cells in synovial biopsies from human osteoarthritis (OA) and rheumatoid arthritis (RA) patients (Zhang et al., 2019). OA and leukocyte-poor RA patients are considered as non- or less inflammatory, whereas leukocyte-rich RA patients show the highest inflammation score. Interestingly, we observed reduced levels of *Rinl* in T cells of leukocyte-rich RA patients as compared with the non-inflammatory OA cohort, while *Cxcr5* expression is highest in leukocyte-rich RA patients (Fig. 10 G). These data indicate that Rinl expression might be beneficial in the disease outcome of RA as it negatively regulates Tfh differentiation, the driving factor of the disease (Ma et al., 2012).

Discussion

Tfh are the crucial components of humoral immunity. To date, numerous positive and negative regulators including TFs, surface receptors, cytokines, ubiquitin ligases, and microRNAs were identified as critical components during the multifactorial and multistep process of Tfh differentiation (Jogdand et al., 2016). However, scientific efforts still focus on identifying more factors with the aim to harness Tfh for novel therapeutics and vaccine development.

This study is the first report of the Rinl-KO mouse model, and we demonstrate that the novel GEF Rinl is an important determinant of Tfh cell differentiation. We identified that Rinl controls Tfh generation under homeostatic conditions, after immunizations with Th2 and Th1/Th17 driving adjuvants, in acute viral infection, during aging, and also in human CD4⁺ T cells. Therefore, Rinl is not regulating Tfh in a particular setting or species but affects Tfh in general. This places Rinl as a universal negative regulator of Tfh cells independently of their subset generation and specification. This is in contrast to other Tfh regulators, for instance, in mice transgenic for an activated

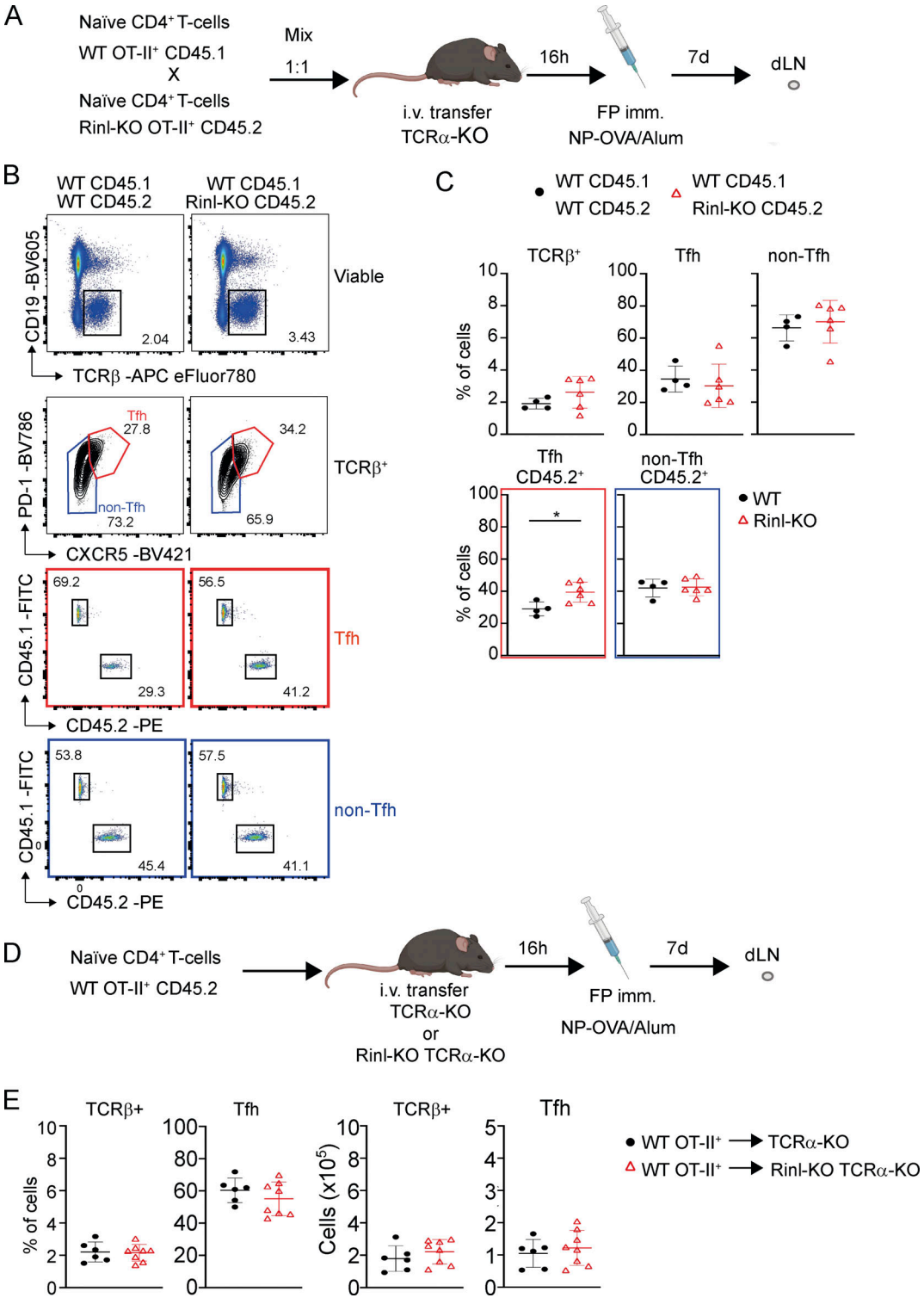

Figure 6. **T cell trans effects do not affect Tfh differentiation in the absence of Rinl. (A)** Experimental scheme. **(B)** Representative flow cytometry plots of TCRβ+ cells, Tfh/non-Tfh, and CD45.1/CD45.2 frequencies among Tfh and non-Tfh. **(C)** Summary of B. Numbers indicate the percentage of cells in the respective gate (B). **(D)** Experimental scheme. **(E)** Summary graphs show percentages and cell counts of TCRβ+ cells and Tfh in TCRα$^{-/-}$ or Rinl$^{-/-}$ TCRα$^{-/-}$ mice. Data show a summary four to six mice (C) or six to eight (E) mice per group analyzed in two independent experiments. Mean ± SEM are shown along individual data points in the graphs. Data were statistically analyzed using unpaired two-tailed *t* tests. *P < 0.05.

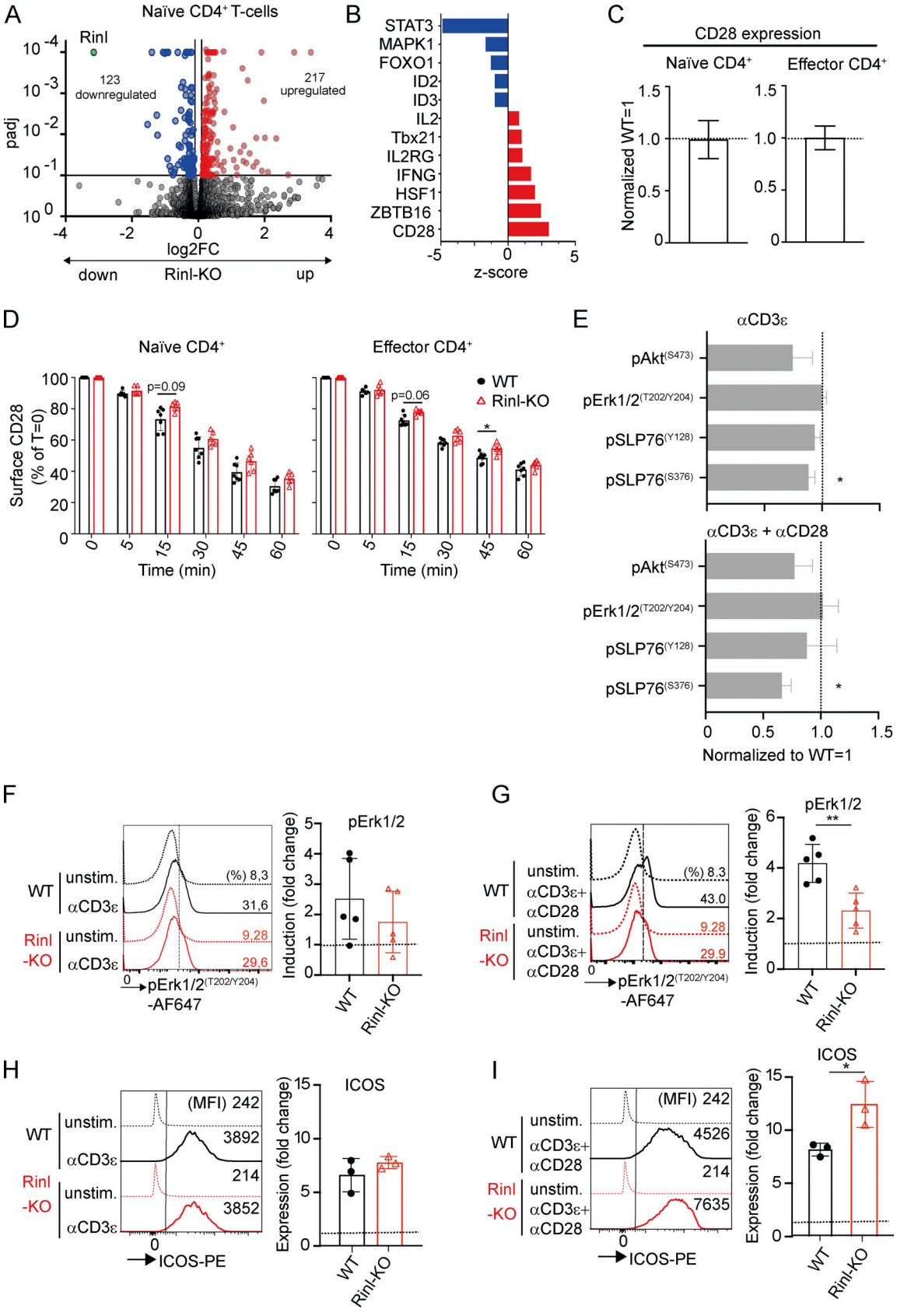

Figure 7. **CD28 trafficking and signaling pathway is regulated by Rinl.** RNA was isolated from sorted WT and Rinl-KO naïve CD4+ T cells (CD62L+CD44−) and subjected to RNA-seq. **(A)** Volcano plot depicts the comparison of global gene expression profiles between WT and Rinl-KO naïve CD4+ T cells. The y axis indicates adjusted P values (−log10), and the x axis shows the $\log_2$ fold change. **(B)** Diagram shows the top dysregulated upstream regulators identified by

Ingenuity Pathway Analysis (Qiagen). Regulators are plotted on y axis and are predicted to be upregulated (positive z-score, red) or downregulated (negative z-score, blue) in Rinl-KO naïve CD4+ T cells. **(C)** The summary graph shows CD28 expression. **(D)** Summary of CD28 internalization kinetic in naïve and effector CD4+ T cells. Internalization was calculated as percentage (%) of CD28 expression from time point 0 (T = 0). **(E)** Summary of phosphorylation of signaling molecules 2 min after αCD3ε or αCD3ε and αCD28 stimulation of CD4+ T cells. **(F)** Representative histograms of $Erk1/2_{(pT202/pY204)}$ of WT and Rinl-KO CD4+ T cells activated with immobilized αCD3 for 48 h are shown. Summary is depicted alongside. **(G)** Representative histograms of $Erk1/2_{(pT202/pY204)}$ of WT and Rinl-KO CD4+ T cells activated with immobilized αCD3+αCD28 for 48 h are shown. Summary is depicted alongside. **(H)** Representative histograms of ICOS surface expression of WT and Rinl-KO CD4+ T cells activated with immobilized αCD3 for 48 h are shown. Summary is depicted alongside. **(I)** Representative histograms of ICOS surface expression of WT and Rinl-KO CD4+ T cells activated with immobilized αCD3 +αCD28 for 48 h are shown. Summary is depicted alongside. Data show a summary of 6 (C), 6–7 (D), 3–4 (E), 5 (F and G), and 6 (H and I) mice per group analyzed in 3–4 (C–E), 5 (F and G), or 3 (H and I) independent experiments. Mean ± SEM are shown along individual data points in the graphs. Data were statistically analyzed using two-way ANOVA using Tukey multiple comparison's test (D). For the comparison of the relative geometric mean fluorescence intensity values between WT (set as 1) and Rinl-KO, WT-normalized KO data points were tested against the null hypothesis that the WT-normalized KO mean is 1, which would signify no change between WT and KO. The dotted line indicates the values corresponding to 1 on the y or x axis. After normalization, the KO data points were tested with a one-sample *t* test (C and E). For F–I, the unstimulated controls were normalized to 1, and a paired two-tailed *t* test was performed with normalized WT and KO data point means corresponding to each individual experiment. The dotted line represents the value 1 used for normalization. *P < 0.05, **P < 0.01.

PI3Kδ where Tfh differentiation was enhanced at baseline and in response to immunization, but not in an acute LCMV infection setting (Preite et al., 2019). Moreover, a series of adoptive transfer experiments clearly indicate that Rinl dampens Tfh differentiation in a T cell–intrinsic manner without affecting their survival, in vivo expansion, or migration capacity. Bcl6 expression levels were not altered in the absence of Rinl, even if more CXCR5+Bcl6+ Tfh cells were generated. This suggests that Rinl downmodulates Tfh commitment in cells that have received stimuli to polarize into Tfh cells. Importantly, in vitro as well as in vivo during immunization studies or viral infection experiments, other Th subsets, such as Th1, Th2, Th17, or Treg, are not affected in the absence of Rinl, revealing that Rinl acts specifically on Tfh differentiation.

Table 1. **Gene list corresponding to the STAT3 upstream regulator**

Symbol	Entrez gene name
CASP1	Caspase 1
CCL5	CC-chemokine ligand 5
CCND2	Cyclin D2
CDKN1B	Cyclin dependent kinase inhibitor 1B
CMPK2	Cytidine/Uridine monophosphate kinase 2
FOXP3	Forkhead-box-protein P3
GBP5	Guanylate binding protein 5
GBP6	Guanylate binding protein 6
HLA-DRB5	Major histocompatibility complex, class II, DR beta 5
IFI16	IFN gamma inducible protein 16
IFIT1	IIFN induced protein with tetratricopeptide repeats 1
IFIT1B	IFN induced protein with tetratricopeptide repeats 1B
IFIT3	IFN induced protein with tetratricopeptide repeats 3
Igtp	IIFN gamma induced GTPase
IRF7	IFN regulatory factor 7
Irgm1	Immunity related GTPase M
ISG15	ISG15 ubiquitin like modifier/IFN, alpha-inducible protein
Klrk1	Killer cell lectin like receptor K1
PIM1	Proto-oncogene serine/Threonine-protein kinase Pim-1
RSAD2	Radical S-adenosyl methionine domain containing 2
SLFN13	Schlafen family member 13
TAP1	Transporter 1, ATP binding cassette subfamily B member
Tgtp1/Tgtp2	T cell specific GTPase 1/2
USP18	Ubiquitin specific peptidase 18

Genes in bold are known to be type I IFN regulated.

Mechanistically, we identified that Rinl acts via controlling CD28 signaling placing it as a new factor in CD28 biology. We cannot fully exclude other functions of Rinl in CD4+ T cells and other immune cells, in particular, as we found STAT3 to be one of the most prominent upstream regulators. Most of the observed gene expression changes connected to STAT3 are related to regulatory functions via type I IFNs. Future studies will aim at understanding the role of Rinl in type I IFN signaling in CD4+ T cells and beyond. However, our findings taken altogether unravel a strong link between Rinl, CD28, and Tfh differentiation. Several studies have demonstrated the central role of CD28 co-stimulation in Tfh generation and as a consequence GC establishment and humoral immune response (Ferguson et al., 1996; Lane et al., 1994; Linterman et al., 2014; Weber et al., 2015). We demonstrate that Rinl dampens CD28 internalization and that after short-term and long-term activation of cells with αCD3ε and αCD28, phosphorylation of downstream molecules is altered. After short-term activation, we detected reduced phosphorylation of SLP76 at Ser376, which was shown to negatively regulate T cell receptor signaling (Di Bartolo et al., 2007). The effect is stronger in cells stimulated with αCD3ε and αCD28 compared to cells solely activated with αCD3ε, suggesting that in the absence of Rinl, TCR signaling was not dampened as strongly by CD28 costimulation. It is therefore tempting to hypothesize that Rinl is rewiring CD28-specific signaling pathways, which orchestrate Tfh differentiation by acting on the CD28 internalization rate.

Following long-term activation of cells with αCD3ε and αCD28 for 48 h, Erk1/2 phosphorylation was reduced in Rinl-KO CD4+ T cells when CD28 costimulation was present. This is an important observation, as a recent study showed the requirement for suppression of CD28-mediated Erk1/2 activation at a later stage of T cell activation for Tfh differentiation (Wan et al., 2021). CD28 nucleates different signaling pathways, which need

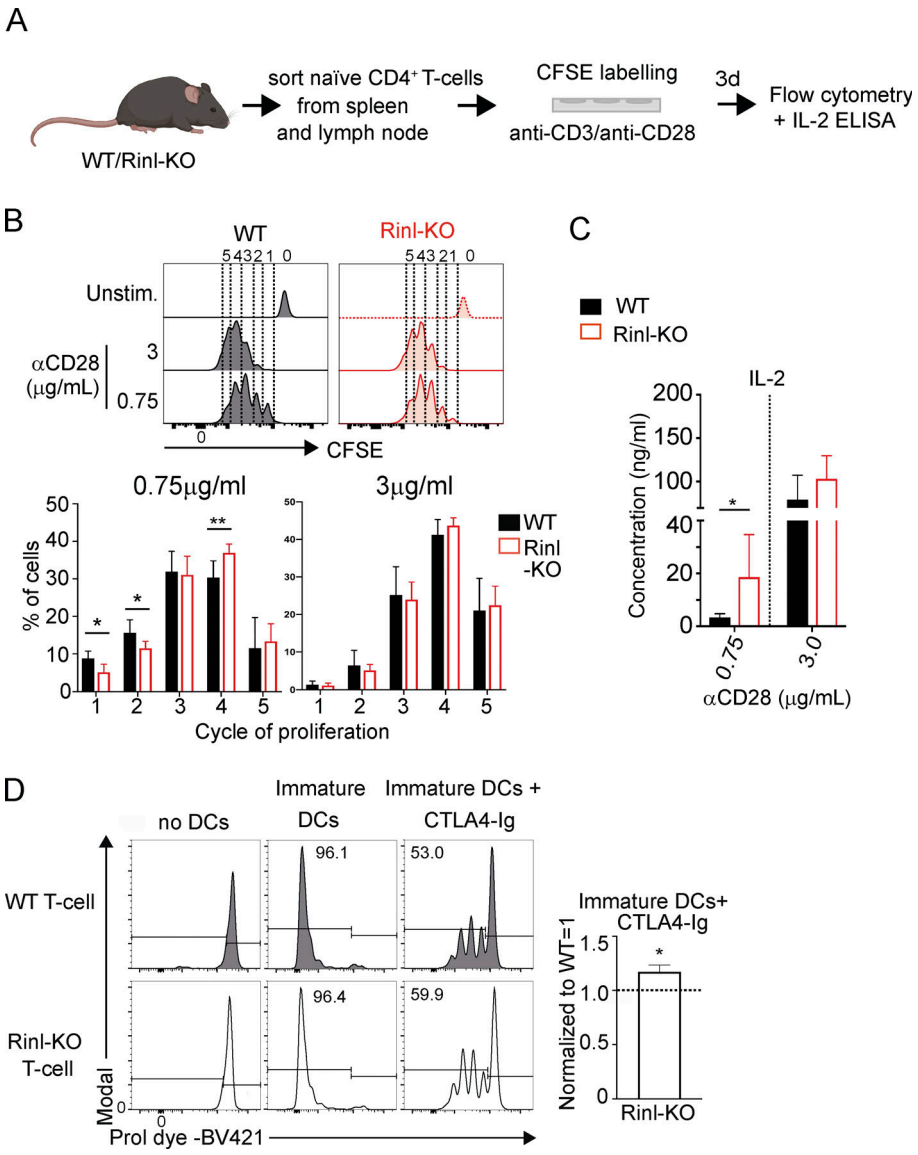

Figure 8. **Rinl controls CD28 signaling strength. (A)** Experimental scheme. **(B)** Representative histograms of proliferation after activation of naïve CD4+ T cells with low (0.75 μg/ml) and high (3 μg/ml) αCD28 for 3 d. Summary of data is shown below. **(C)** Summary of IL-2 measured from supernatants of cells cultured as in B. **(D)** Representative histograms depicting proliferation of T cells after activation with BMDCs ± CTLA4-Ig. Summary is shown alongside. Six (B and C) and three (D) mice per group were analyzed in three to four (B–D) independent experiments. P values were calculated by two-way ANOVA using Tukey multiple comparison's test (B). Mean ± SEM are shown in the graphs. Data were statistically analyzed using unpaired two-tailed *t* test (C). For the comparison of the relative frequencies of divided cells between WT (set as 1) and Rinl-KO, WT-normalized KO data points were tested against the null hypothesis that the WT-normalized KO mean is 1, which would signify no change between WT and KO. The dotted line indicates the values corresponding to 1 on the y axis. After normalization, the KO data points were tested with a one-sample *t* test (D). *P < 0.05.

to be orchestrated at multiple stages and correctly timed to induce a particular Th specification, and we describe here a previously unrecognized mechanism by which Rinl regulates these events. Namely, Rinl acts via an SLP76-dependent pathway early in CD28 signaling and via dampening of Erk1/2 at a later stage, a regulation that matches the multistage differentiation requirements of Tfh cells.

Seminal studies have established that ICOS expression is induced by TCR stimulation and its high expression is dependent on CD28 co-stimulation (McAdam et al., 2000). We observed higher ICOS expression and an increased frequency of ICOS+ cells after in vitro activation of Rinl-KO naïve CD4+ T cells upon anti-CD3 and anti-CD28 stimulation together but not with anti-CD3 stimulation alone, reinforcing our hypothesis that Rinl shapes CD28 signaling. In addition, it was shown that CD28 is crucial for early Tfh commitment, inducing a Tfh program within 2–4 d after the onset of the immune response, whereas ICOS was shown to be critical for Tfh cell maintenance at later time points (Weber et al., 2015). The observation of a stronger Tfh commitment in the absence of Rinl as early as 48 h after immunization in our adoptive transfer experiments reinforces our hypothesis that Rinl acts rather via CD28 than ICOS. Altered CD28 signaling leading to increased ICOS levels in the absence of Rinl might further contribute to the increase in Tfh cell frequencies in vivo. Consistent with this model, we indeed observed an increased ICOS expression and frequency of ICOS+ Tfh cells in the absence of Rinl also in vivo after adoptive transfer experiments.

Another important finding of our study is that Rinl has an effect on CD28 signaling strength. Rinl-KO cells displayed increased proliferation and IL-2 production with low anti-CD28 concentrations compared with WT cells but not at high αCD28 concentration. Interestingly, Rinl-KO CD4+ effector and Tfh cells secreted more IL-2 in vivo, indicating that our in vitro observations correlate with in vivo Th differentiation. This is of high interest as CD4+ T cells that are IL-2 producers were shown to differentiate into Tfh cells establishing IL-2 production as an early marker for cell fate determination towards this helper

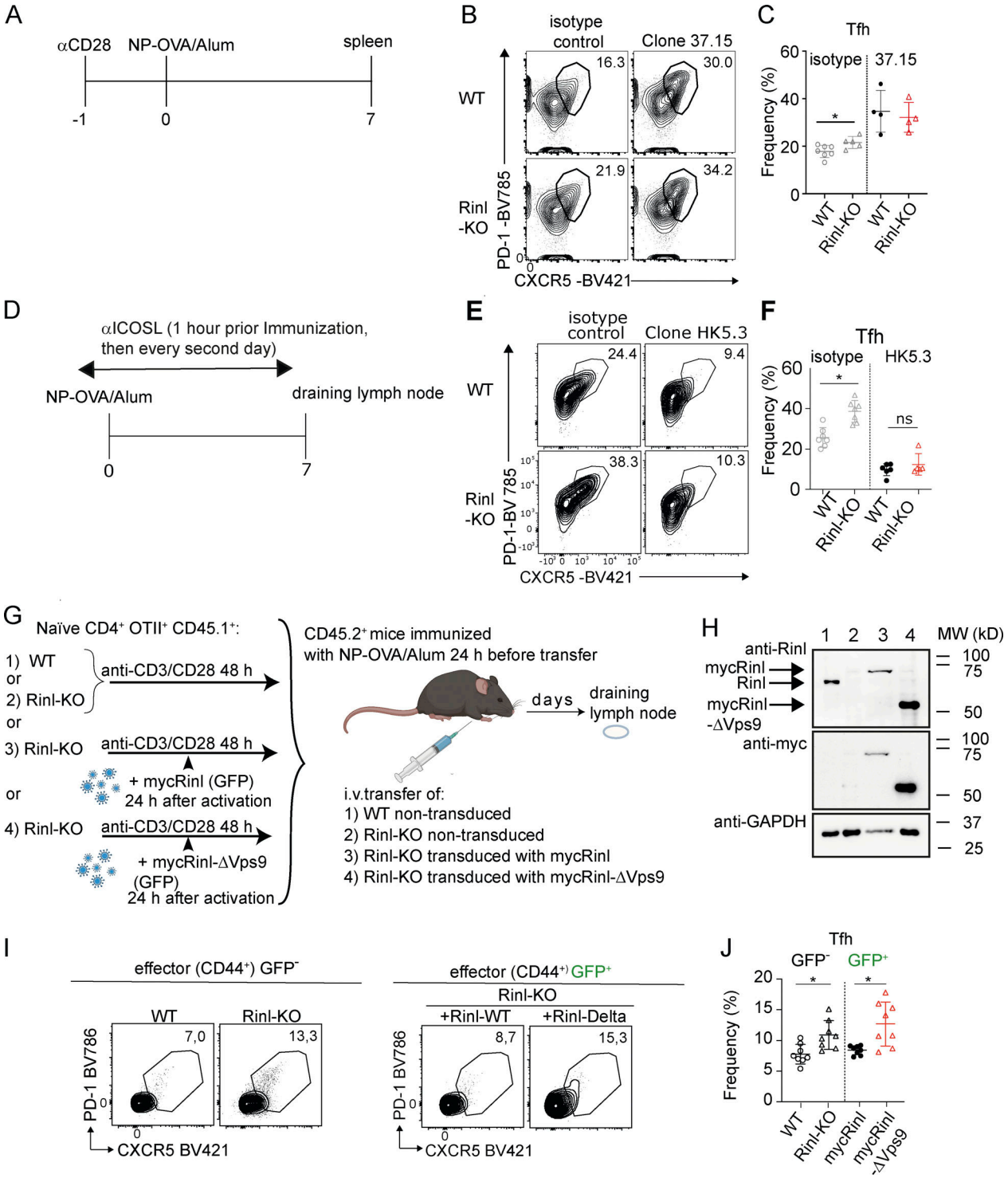

Figure 9. **The GEF function of Rinl is required to restrain Tfh differentiation in vivo via CD28. (A)** Experimental scheme. **(B)** Representative contour plots of Tfh of WT and Rinl-KO mice treated with isotype control or αCD28 (Clone 37.15) 1 d before immunization. **(C)** Summary of B. **(D)** Experimental scheme. **(E)** Representative contour plots of Tfh of WT and Rinl-KO mice treated with isotype control or αICOSL (Clone HK5.3) 1 h before immunization and then every second day. **(F)** Summary of E. **(G)** Experimental design showing the retroviral transduction of mycRinl and mycRinl-ΔVps9 into Rinl-KO OTII+ naïve CD4+ T cells prior to adoptive transfer into congenic mice. Non-transduced activated WT and Rinl-KO cells were used as control. Congenic mice were immunized into the FP with NP-OVA/alum 24 h prior to adoptive T cell transfer. **(H)** Rinl protein expression was monitored by SDS-PAGE 48 h after transduction. GAPDH was used as loading control. **(I)** Representative contour plots of Tfh in dLN of congenic recipient mice treated as described in G 7 d after immunization. **(J)** Summary of I. Data represent 4–7 (C), 6 (F), and 8 (J) mice per group in two independent experiments. Mean ± SEM are shown along individual data points in the graphs. P values were calculated using an unpaired two-tailed *t* test. *P < 0.05. Source data are available for this figure: SourceData F9.

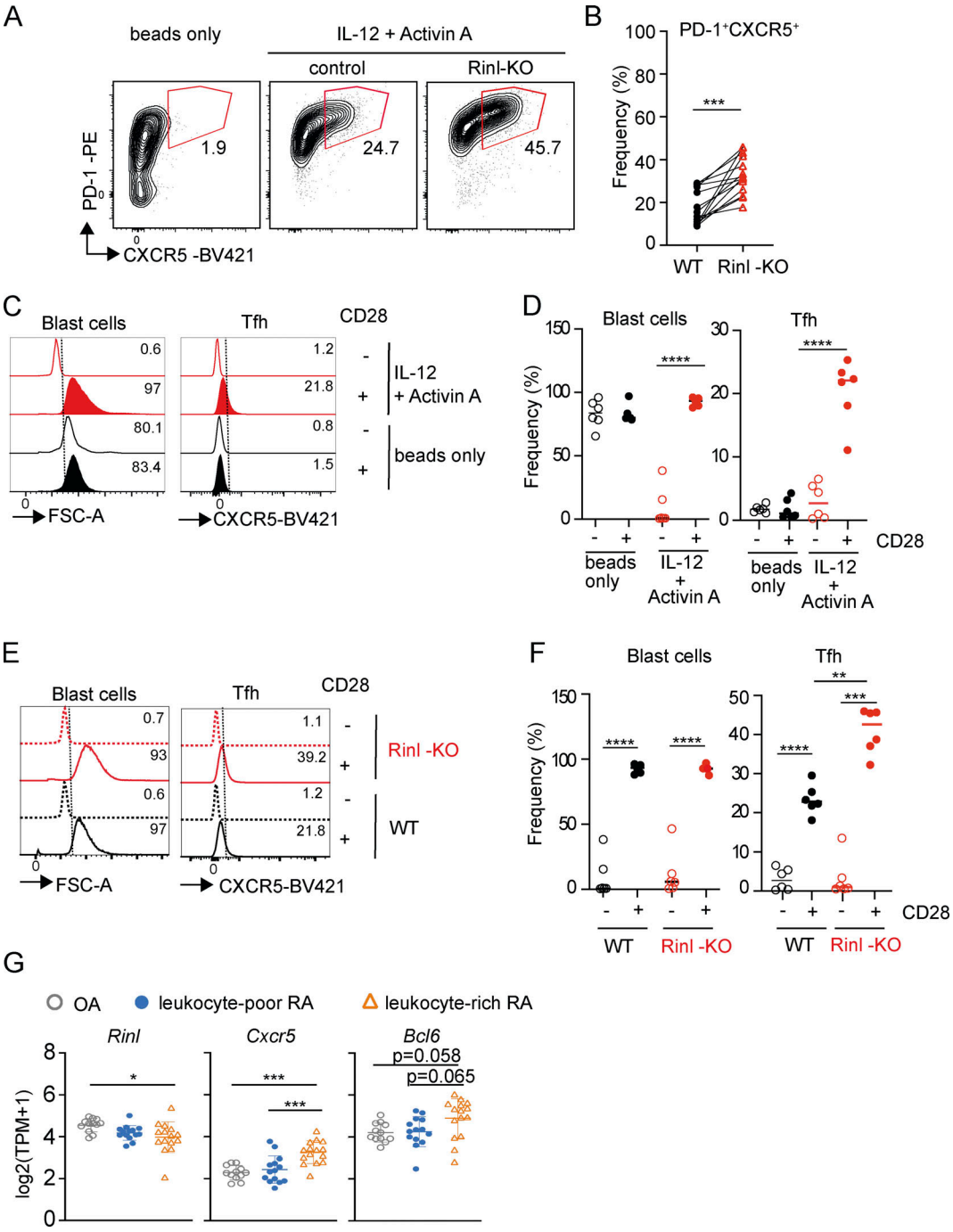

Figure 10. **Rinl negatively regulates Tfh differentiation in human CD4⁺ T cells. (A)** Representative contour plots showing human PD-1⁺CXCR5⁺ Tfh cells. Rinl was knocked-out in human CD4⁺ T cells and control and Rinl-KO cells were subsequently cultured under Tfh-skewing conditions for 5 d. **(B)** Summary of data shown in A. **(C)** Histograms represent the size and CXCR5 expression of human naïve CD4⁺ T cells cultured for 6 d with αCD3 or αCD3/αCD28 coated beads in the absence or presence of Tfh-skewing cytokines. **(D)** Summary of C. **(E)** Rinl was knocked-out in human CD4⁺ T cells by CRISPR-Cas9 technology and control and Rinl-KO cells were subsequently cultured as in C under Tfh skewing conditions. Histograms represent the size and CXCR5 expression of the cultured cells. **(F)** Summary of E. **(G)** *Rinl*, *Cxcr5*, and *Bcl6* expression in T cells retrieved from synovial biopsies of different patient cohorts (Zhang et al., 2019). TPM, transcripts per million. Data show a summary of 14 donors (B) and 8 donors (D and F) analyzed in four independent experiments (B) and two independent experiments (D and F). Mean ± SEM are shown along individual data points in the graphs. Data were statistically analyzed using paired two-tailed *t* tests (B) or one-way ANOVA analysis followed by Tukey's multiple-comparisons test (D, F, and G). *P < 0.05, **P < 0.01, ***P < 0.001, ****P < 0.0001.

subset (DiToro et al., 2018). As we were performing our in vitro studies without the addition of Tfh-driving cytokines such as IL-6 or IL-21 (Suto et al., 2008), this is a strong indication that in the absence of Rinl, CD4⁺ T cells gain a higher Tfh differentiation potential due to alterations in CD28 signaling strength. We cannot rule out that despite overall normal T cell development, the strength of the TCR signal might also be altered in Rinl-KO mice due to alterations in the TCR repertoire, leading to the

selection of T cells with stronger peptide-MHC binding capacity, which have been shown to preferentially skew toward Tfh (Fazilleau et al., 2009; Tubo et al., 2013). In line with this concept are our observations that frequencies of effector CD4⁺ T cells are enhanced in the absence of Rinl in homeostatic conditions. Further studies will focus on elucidating the TCR repertoire in Rinl-KO mice. However, our adoptive transfer experiments based on a clonal OTII TCR show additional mechanisms besides TCR signaling strength.

In addition, to study whether the alterations in CD28 endocytosis and signaling are relevant in Tfh differentiation in vivo, we aimed to rescue our phenotype by providing additional CD28 stimulation. Interestingly, we were indeed able to achieve the same frequencies of Tfh after treatment with αCD28 in WT and Rinl-KO mice, suggesting that the dysregulation of the CD28 pathway also plays a role in vivo. In summary, our mechanistic studies indicate that the regulation of Tfh differentiation by Rinl operates via modulation of CD28 function in vitro and in vivo.

We also uncovered that the GEF function of Rinl was required to restrain Tfh differentiation in vivo, implying that Rinl regulates CD28 endocytosis via GEF-dependent mechanisms. Indeed, Rinl was identified as a GEF specific for Rab22 and Rab5a, which are important regulators of early endocytosis in clathrin-dependent and -independent pathways, endosome fusion, and endosome trafficking (Stenmark, 2009). CD28 internalization was described to occur via clathrin-dependent mechanisms (Badour et al., 2007). It is therefore tempting to speculate that Rinl connects Rab5-dependent functions to CD28-specific internalization in CD4⁺ T cells, which shape CD28 signaling and restrain Tfh differentiation.

Genetic variants at the CD28 locus are associated with RA (Raychaudhuri et al., 2009), underscoring the importance of the CD28 pathway as a gatekeeper of proper immune responses. Of note, Rinl had a lower expression in cells from leukocyte-rich synovial fluids of RA patients which also showed increased Tfh hallmarks compared with cells from synovial fluids of patients with less inflammatory phenotype. This indicates that Rinl might control the differentiation of Tfh during RA and suggests it as a biomarker of this specific disease, opening new directions of investigation. Therefore, our study has also an important implication for therapeutic considerations.

Finally, various studies indicate that angioimmunoblastic T cell lymphoma, a subtype of peripheral T cell lymphomas, is derived from Tfh (de Leval et al., 2007; Roncador et al., 2007), and angioimmunoblastic T cell lymphoma is associated with two recurrent mutation sites of CD28 (Rohr et al., 2016). It was proposed that these mutations tune CD28 signaling by affecting CD28 endocytosis. Consequently, CD28 endocytosis might be a central regulatory mechanism on how CD4⁺ T cells control Tfh differentiation and further oncogenicity/malignancy. Therefore, our study highlights a novel regulator of Tfh differentiation and in addition a potential novel regulatory mechanism driving Th fate decision based on CD28 endocytosis. In this light, future studies with CD28 mutants engineered into human CD4⁺ T cells under Tfh differentiation conditions, as well as CD28 endocytosis studies and their consequence on CD28 signaling are warranted.

Taken together, our study provides an in-depth analysis of Rinl function in lymphocyte development, homeostasis, and activation. We reveal a previously unrecognized mechanism by which a GEF controls the differentiation of Tfh in various contexts. Our data provide evidence of how GEF function might regulate the generation of Th cells by controlling receptor trafficking in homeostasis and upon activation and may, if dysregulated, lead to disease.

Limitations of our study

Our study showed how a novel GEF involved in endocytic processes regulates Tfh differentiation in vitro and in vivo in a T cell–intrinsic way by regulating CD28 endocytosis and signal transduction. Due to the lack of specific antibodies against murine Rinl and technical limitations in visualizing intracellular compartments in murine primary CD4⁺ T cells, our study did not address whether Rinl and CD28 directly interact or colocalize in the same intracellular compartment after endocytosis. The generation of suitable anti-Rinl antibodies for confocal microscopy will be the focus of future approaches and will be key for further mechanistic studies.

Conclusion

Our study identifies Rinl as a key negative regulator of Tfh cell differentiation. Our conclusion that Rinl controls Tfh differentiation via CD28 signaling is based on the following observations: (i) RNA-seq data revealed CD28 as a major dysregulated upstream regulator in Rinl-KO CD4⁺ T cells. (ii) In vitro, pErk1/2$^{(T202/Y204)}$ was more reduced and ICOS expression was more enhanced in the absence of Rinl only when CD28 signals were present. Since reduced Erk phosphorylation via CD28 (Wan et al., 2021) and high ICOS expression (Crotty, 2011; McAdam et al., 2000; Rasheed et al., 2006; Weber et al., 2015) are key determinants for Tfh differentiation, these data strengthen the proposed regulation of Tfh cells by Rinl via CD28. (iii) In vivo, we observed an increase of Tfh cells as early as 48 h, matching with an altered CD28 signal (Weber et al., 2015). (iv) We observed a higher expression of ICOS on effector and Tfh cells lacking Rinl 7 d after immunization, in line with our in vitro data. (v) The injection of anti-CD28 antibodies enhanced Tfh differentiation in WT CD4⁺ T cells, which resulted in equal Tfh frequencies in WT and *Rinl*$^{-/-}$ mice after immunization, showing that strong CD28 signals in WT CD4⁺ T cells can abolish differences in the KO cells. (vi) CD28 endocytosis was altered in the absence of Rinl in CD4⁺ T cells. Rinl acts as GEF for Rab5 GTPases, which are involved in early endocytic processes, and the GEF activity of Rinl was required to fulfill its inhibitory function on Tfh cell differentiation. Taking all data together, we conclude that Rinl regulates Tfh differentiation via the control of CD28 endocytosis and signaling. However, one cannot formally rule out that Rinl might also regulate the endocytosis of other receptors important for T cell activation and/or Tfh differentiation. Additional experiments investigating CD28 endocytosis in more detail in comparison with other receptors, especially during/after TCR stimulation focusing on the immunological synapse and in more physiological conditions by stimulation with CD80 or CD86 are warranted. Of note, we also observed

signaling defects in *Rinl*$^{-/-}$ CD4$^+$ T cells in the absence of CD28 costimulation. For instance, pSLP76$^{(S376)}$ was reduced in the absence of CD28 signal in *Rinl*$^{-/-}$ CD4$^+$ T cells, although the addition of CD28 signals increased the difference. This observation relates to the complexity of TCR/CD28 signaling pathways, which are very intricate and interwoven. Therefore, additional functions of Rinl in T cells independently of controlling CD28 signaling are likely and will be the focus of future investigations by phosphoproteomics including variation of the TCR signaling strength in the absence or presence of variable CD28 signaling levels.

In summary, our study uncovers that Rinl has a crucial role in the regulation of Tfh differentiation by controlling CD28 signaling.

Materials and methods

Mice

Rin-like–deficient mice were generated using a targeting construct containing a STOP codon in the reading frame of exon 4. The STOP codon was followed by the IRES-LacZ::GFP cassette and a floxed neomycin. Subsequently, Rinl$^{+/KI\text{-}neo}$ mice were crossed with CMV-Cre mice to delete neomycin resulting in Rinl$^{+/KI}$ mice.

OT-II TCR transgenic mice were provided by M. Bonelli. TCRα KO mice were kindly provided by Iris Gratz (University of Salzburg, Salzburg, Austria).

CD45.1$^+$ congenic mice were obtained from the European Mouse Mutant Archive (EM:01998).

Rin-like genotyping was performed from toetip DNA via PCR using primers as follows: 5′-TGGAAGATGGGTCCAGCACT-3′; 5′-GCAGCTCCCTTTGCTCTTGA-3′; 5′-GCCACAAGTTCAGCG TGTCC-3′.

All animal experimentation protocols were evaluated by the ethics committee of the Medical University of Vienna and approved by the Federal Ministry for Science and Research, Vienna, Austria. Animal husbandry and experimentation were performed according to the Federation of Laboratory Animal Science Associations guidelines under national laws (Federal Ministry for Economy and Science, Vienna, Austria). These guidelines match those of Animal Research: Reporting of In Vivo Experiments (ARRIVE).

Analyzed mice were of mixed sex and between 8 and 12 wk old unless otherwise stated. Rinl-KO mice were backcrossed 10 times to C57BL/6 background and littermate controls were used in experiments.

Flow cytometric analysis, antibodies, and reagents

The following antibodies and reagents were used in our study: from BD Biosciences: IL-17A-BV785 (RRID: AB_2738642, TC11-18H10.1), CD8a-APC-R700 (AB_2739032, 53-6.7); from ThermoFisher: Bcl6-APC (AB_11042584, BCL-UP), CD4-PE-Cy7 (AB_469578, RM4-5), CD162/PSGL-1-PE (AB_2572585, FLEG), Foxp3-APC (AB_469457, FJK-16 s), IL-21-A647 (AB_2784739, mhalx21), TCRβ-APC-e780 (AB_1272173, H57-597), fixable viability dye eFluor 506; from BioLegend: CD16/CD32 (AB_312801, 2.4G2), CD4-BV785 (AB_2563053, RM4-5), CD8a-PerCP-Cy5.5 (AB_2075238, 53-6.7), CD19-BV605 (AB_2563067, 6D5), CD25-APC (AB_312861, PC61), CD44-A700 (AB_493713, IM7), CD44-BV510 (AB_2650923, IM7), CD44-PerCP-Cy5.5 (AB_2076204, IM7), CD45.1-FITC (AB_313495, A20), CD45.1-PE-Dazzle594 (AB_2564295, A20), CD45.2-PE (AB_313445, 104), CD45.2-APC (AB_389211, 104), CD45.2-PerCP-Cy5.5 (AB_893350, 104), CD62L-APC (AB_313099, MEL-14), CD69-PE-Cy7 (AB_493564, H1.2F3), CD90.2-BV605 (AB_2632889, 30-H12), CD95-PE (AB_2632902, SA367H8), CD185/CXCR5-BV421 (AB_2562128, L138D7), human CD185/CXCR5-BV421 (AB_2562303, J252D4), CD278/ICOS-PE (AB_313335, 15F9), human CD279/PD-1 BV785 (AB_2721562, NAT105), CD279/PD-1 BV785 (AB_2563680, 29F.1A12), GL7-A647 (AB_2562185, GL7), IFNγ-FITC (AB_315400, XMG1.2), IgD-BV421 (AB_2562743, 11-26c.2a), IgG1-FITC (AB_493293, RMG1-1), IL-2-BV605 (AB_11204084, JES6-5H4), IL-4-APC (AB_315320, 11B11), IL-5-APC (AB_315330, TRFK5), Ly-6C-PE-Cy7 (AB_1732082, HK1.4). The clone number is indicated in brackets. I-A^b LCMV GP66-77 (DIYKGVYQKSV) tetramer-PE (National Institutes of Health tetramer facility).

LCMV infection

For infection, 2 × 10^5 PFU LCMV Armstrong strain viruses were injected i.p., and spleens were analyzed 8 or 21 dpi.

Immunization

Antigen mixture for immunization was prepared by mixing OVA$_{(323–339)}$ peptide (Sigma-Aldrich) or NP-OVAL (Ovalbumin; Biosearch Technologies) in PBS and Imject Alum Adjuvant (Thermo Fisher Scientific) while vortexing and afterward rotation for 2–3 h at 4°C. Alternatively, CFA was used as an adjuvant.

Mice were immunized with 100 µg/ml NP-OVA/Alum i.p. For flow cytometry analysis, spleens were harvested on day 7 after immunization.

Subcutaneous FP immunization was performed with 10 µg/ml OVA$_{(323–339)}$/Alum or CFA or 10 µg/ml NP-OVA/Alum in each FP and analysis was done as indicated in figure legends.

For the in vivo CD28 study, 100 µg/ml of anti-mouse CD28 (Clone 37.15; BioXcell) or isotype control (isotype poly Syrian hamster IgG; BioXcell) were injected i.p. 1 d before immunization. For ICOSL blocking experiments, 100 µg anti-mouse ICOSL (Clone HK5.3; BioXcell) or isotype control (rat IgG2a; BioXcell) were injected i.p. in 100 µl 1 h before immunization and afterward every second day for two additional times.

Adoptive T cell transfer

WT OT-II$^+$ CD45.1$^+$, WT OT-II$^+$ CD45.2$^+$, or Rinl-KO OT-II$^+$ CD45.2$^+$ naïve CD4$^+$ T cells were enriched using negative selection with magnetic beads (naïve CD4$^+$ T cell isolation kit; Mitlenyi Biotec) according to the manufacturer's protocol. After washing with PBS, 1 × 10^5–1 × 10^6 naïve (CD62L$^+$CD44L$^-$) OT-II$^+$ CD4$^+$ T cells in 100 µl PBS were injected retro-orbitally into immobilized recipient mice (CD45.1, CD45.1xCD45.2, TCRα-KO, or TCRα-KO Rinl-KO). For analysis of proliferation, cells were labeled with CFSE (Molecular Probes) by incubating 1 × 10^7 cells/ml in PBS with 10 mM CFSE (Molecular Probes) for 10 min at room temperature before injection. Approximately 16 h after

T cell transfer immunization in each FP was performed. dLN, ndLNs, and spleens were analyzed by flow cytometry 2 or 7 d after immunization.

For histology of dLNs, 1×10^6, 2×10^5, or 1×10^5 naïve OT-II$^+$ CD4$^+$ were transferred and dLNs were collected at days 3, 5, and 7 after immunization, respectively.

Isolation and activation/differentiation of CD4$^+$ T cells

CD4$^+$ T cells were isolated from pooled axillary, brachial, and inguinal LN and spleens of WT and Rinl-KO mice. The cell suspensions were incubated with biotinylated anti-CD8α (RRID: AB_312743; 53-6.7), anti-CD11b (AB_312787; MEL1/70), anti-B220 (AB_312988; RA3-6B2), anti–Gr1 (AB_313369; Ly-6g), anti-Ter119 (AB_313705; Ter-119), anti-CD11c (AB_313773; N418), and anti-NK1.1 (AB_313391; PK136) Antibodies in PBS supplemented with 2% FBS. Antibodies were purchased from BioLegend. Subsequently, CD4$^+$ T cells were pre-enriched by magnetic negative depletion using streptavidin beads (MagniSort SAV Negative Selection beads; Thermo Fisher Scientific) according to the manufacturer's description. For total CD4$^+$, cells were used immediately. For naïve CD4$^+$ T cells, pre-enriched CD4$^+$ T cells were stained and sorted for CD25$^-$ CD44^{low}CD62L$^+$ on a SH800 (SONY).

For in vitro activation studies, purified naïve CD4$^+$ T cells were labeled with CFSE or cell Proliferation Dye eFluor 450 (eBioscience) by incubating 1×10^7 cells/ml in PBS with 10 mM CFSE for 10 min at room temperature. The labeling reaction was stopped by adding T cell medium. Afterward, 1×10^5 cells in 200 µl/well complete T cell medium (RPMI 1640 supplemented with 10% FCS [Sigma-Aldrich/Biowest], antibiotics [PenStrep], Glutamax, 50 mM βME) were seeded on 96-well flat-bottom plates. The plates were precoated overnight with 1 µg/ml anti-CD3ε (AB_394590; BD Biosciences) and different anti-CD28 (AB_394763; BD Biosciences) concentrations. Cells were harvested and analyzed on day 3. Additionally, supernatant was kept for analysis of IL-2.

Th1/Th17 and iTreg cells were generated from sorted naïve CD4$^+$ T cells activated with 1 µg/ml anti-CD3ε/anti-CD28 for 3 d in a complete T cell medium supplemented with different cytokine mixes. For Th1 condition, 5 ng/ml IL-12 (R&D Systems), 20 U/ml rhIL-2 (PeproTech), and 3 µg/ml anti–IL-4 (BioXcell) were used. For Th17 condition 20 ng/ml IL-6, 1 ng/ml rhTGF-β1 (BioLegend), 10 ng/ml IL-1β (BioLegend), and 20 ng/ml IL-23 (R&D Systems) were used, and for iTreg condition, 1 ng/ml rhTGFβ1. Th2 cells were generated by activating naïve CD4$^+$ T cells with 1 µg/ml anti-CD3ε/3 µg/ml anti-CD28 for 3 d in complete T cell medium supplemented with 250 U recombinant IL-4 (PeproTech), 6 µg/ml anti-IL-12 (BioXcell), 10 µg/ml anti-IFNγ (BioXcell), and 10 U/ml rhIL-2 (PeproTech). After 3 and 5 d, cells were split, and fresh blocking antibodies were added. Cells were analyzed on day 6.

Plasmids

Full-length and ΔVps9 (aa 1–394) Rinl carrying an N-terminal myc-tag (Woller et al., 2011) were subcloned into a murine stem cell virus–based retroviral vector containing the IRES-GFP cassette (pMIGR).

Transduction of naïve OTII$^+$ CD4$^+$ T cells

Retroviral vector (20 µg) transfection was performed when Phoenix-E packaging was 60–70% confluent in 10-cm dishes by using standard calcium phosphate precipitation. Medium was changed 6–8 h after transfection. 1 d after transfection, the medium was changed to complete RPMI 1640 medium. Viral supernatants were collected on the following day, filtrated through a 0.45-µm filter, and used for the infection of pre-activated (24 h) CD4$^+$ T cells. The transduction was performed by adding 1 ml virus and polybrene (10 µg) containing supernatant to the activated T cells. The cells were centrifuged at 600 *g* for 2 h at 32°C. After spin infection, the cells were placed for 1 h at 37°C and 5% CO_2. After this incubation, the medium was changed to T cell medium and the cells were further cultured for 24 h prior to transfer into immunized mice or 48 h to assess transduction efficiency by immunoblotting using antibodies against Rinl (Woller et al., 2011), myc (Sigma-Aldrich) and GAPDH (Cell Signaling).

CRISPR-Cas9 mediated deletion of Rinl in human CD4$^+$ T cells and human Tfh culture

All functional assays were performed in IMDM (Gibco, Thermo Fisher Scientific) supplemented with 10% of FCS (Gibco) and 10 µg/ml of gentamycin (Gibco). Peripheral blood draws were performed from healthy human volunteers in accordance with the Ethics Committee of the Medical University of Vienna (EC number EK 1150/2015). Mononuclear cells were isolated by standard Ficoll-Paque centrifugation. Naïve human CD4$^+$ T cells were isolated using the EasySep Human Naïve CD4$^+$ T cell Isolation Kit II (Stem Cell Technologies) according to the manufacturer's instructions. The purity of isolated cells was assessed by flow cytometry and found >95% for all specimens. Subsequently, CRISPR-Cas9 knockout of human Rinl was performed as described before (Seki and Rutz, 2018). In detail, 1 µl of a mixture of two Rinl-specific CRISPR RNAs (crRNAs; Alt-R CRISPR-Cas9 crRNA; total concentration 320 µM; sequences: 5′-TGGACCCTGCCGATCTGCACAGG-3′; 5′-TGAATGGTGAGC ACGTCCTCAGG-3′; underlined is PAM sequence) were mixed with 1 µl tracrRNA (320 µM; all Integrated DNA Technologies) and hybridized for 10 min at room temperature. The crRNA–tracrRNA duplex was subsequently complexed with 0.7 µl recombinant Cas9 (Alt-R S.p. Cas9 Nuclease V; 10 µg/µl; IDT) for 30 min at 37°C. Similarly, a control RNP complex was assembled using a non-targeting crRNA (Alt-R CRISPR-Cas9 Negative Control crRNA #1; IDT). For electroporation, 1×10^6 purified naïve T cells were resuspended in 15 µl buffer P3 + 5 µl Supplement 1 (P3 Primary Cell 4D-Nucleofector X Kit S; Lonza) and mixed with 2.7 µl RNP in the 16-well strips provided in the kit. Cells were electroporated on a 4D nucleofector (4D-Nucleofector Core Unit, 4D-Nucleofector X Unit; Lonza) using the pulse code EH100. Immediately afterwards, 80 µl prewarmed fresh medium was added to the cells. After 1 h of resting, cells were transferred to 24-well plates and incubated for 3 d in a medium containing 10 U/ml rhIL-2 (Peprotech) to allow the establishment of the knockout. CRISPR-Cas9 knockout efficiency was determined by Sanger sequencing of the target sites of the two guide RNAs and analyzed using the Synthego inference of

CRISPR edits analysis tool (ICE v2 CRISPR Analysis Tool; Synthego), and the knockout score defining frameshift insertions/deletions was found to be >50% for both loci in all samples tested.

Human Tfh culture was performed as described previously (Locci et al., 2016) using the human T-activator CD3/CD28 dynabeads (Thermo Fisher Scientific).

Preparation of anti-CD3 and anti-CD3/CD28 coated beads

4×10^7 goat anti-mouse IgG dynabeads (Thermo Fisher Scientific) were incubated in 500 µl of Cell Sort Buffer (CSB: PBS, 2% FCS and 1 mM EDTA) with 5 µg/ml anti-human CD3 Antibody (AB_11150592, OKT3) alone or together with 5 µg/ml anti-human CD28 antibody (AB_11148949, CD28.2). After 30 min incubation at room temperature, the beads were washed with CSB and resuspended in T cell medium to a concentration of 2×10^7 beads/ml. Human Tfh culture was performed with these beads as described previously (Locci et al., 2016).

Extracellular and intracellular stainings

Thymii, spleens, peripheral LNs, and PP were removed and passaged through a 70-µm nylon cell strainer to receive single-cell suspension. Erythrocytes were removed by using Pharmlyse (BioLegend). 2×10^6 cells were incubated with Fc block (BD Pharmingen) and subsequently stained for surface markers with fluorophore-conjugated antibodies for 30 min on ice.

For intracellular TF staining, cells were fixed and permeabilized using the FoxP3 staining buffer set (Thermo Fisher Scientific) according to the manufacturer's protocol. For intracellular cytokine staining, cells were stimulated with phorbol 12-myristate 13-acetate (PMA; 25 ng/ml) and ionomycin (750 ng/ml; both Sigma-Aldrich) in the presence of GolgiStop (4 µl/6 ml; BD Biosciences) for 3–4 h. Cells were then fixed/permeabilized using Cytofix/Cytoperm (BD Biosciences). Measurements were performed with a BDFortessa and analyzed using FlowJo 10.2 software (TreeStar).

Phospho staining

Intracellular staining of $pSLP76_{Ser376}$, $pSLP76_{Y128}$, $pErk1/2_{T202/Y204}$, and $pAkt_{S473}$ of activated $CD4^+$ T cells was performed by fixing for 15 min at 37°C with BD Cytofix (BD Biosciences), permeabilization for 30 min on ice with BD Phosflow Perm Buffer III (BD Biosciences), and staining with the indicated phospho antibodies in PBS/2% FCS for 1 h in the dark at 4°C.

Short-term activation assay

For short term activation, 0.5×10^6 $CD4^+$ T cells were incubated with biotinylated 1 µg/ml anti-CD3ε (Clone 145-2C11; BioLegend) alone or in combination with 2 µg/ml biotinylated anti-CD28 (Clone 37.15; BioLegend) for 15 min at room temperature. Streptavidin (1 µg/ml) was added and samples were transferred to 37°C for 2 min. The reaction was stopped by the addition of Cytofix and subsequent staining with phosphor-antibodies.

Confocal microscopy of dLNs

dLNs were harvested and fixed in Antigenfix (Diapath) for 1.5 h, washed with PBS, and then dehydrated in 30% sucrose prior to embedding in optimal cutting temperature compound freezing media (Bio-Optica). 20 µm sections were cut on a CM1520 cryostat (Leica) and adhered to Superfrost Plus slides (Thermo Fisher Scientific). Sections were then blocked in PBS containing 0.3% Triton X-100 (Sigma-Aldrich) and 0.5% BSA followed by incubation with Fc block in the same blocking buffer. The following primary antibodies were used for staining: BV421-conjugated anti-CD45R/B220 (RA3-6B2; BioLegend), AF488-conjugated anti-CD45.2 (104; BioLegend), biotinylated anti-LYVE-1 (ALY7; eBiosciences), BV421-conjugated anti-TCRβ (H57-597; BioLegend), and biotinylated CD21/35 (7E9; BioLegend). The following secondary antibodies were used for staining: Streptavidin, Alexa Fluor 555, or Alexa Fluor 647 Conjugate (Invitrogen). Images were acquired on an inverted Leica microscope (TCS STED CW SP8; Leica Microsystems). A motorized stage was used for tiled imaging. Image analysis was performed using Imaris Microscopy Image Analysis Software (Version9.1.2; Oxford Instruments).

Internalization assay

Internalization assay was performed as previously described with minor changes (Finetti et al., 2014). Shortly, 2×10^6 $CD4^+$ T cells were seeded out in 96-well round-bottom plates (Sarstedt) and incubated with 1 µg/ml biotinylated anti-CD28 antibody (Clone 37.15; BioLegend) PBS + 2% FCS for 30 min on ice to allow binding. After washing steps, cells were incubated at 37°C to induce endocytosis. 30 µl of the cell suspension was transferred immediately into a new plate on ice (time point = 0). Subsequently, aliquots were collected at different time points and internalization was stopped by incubating the cells on ice. Samples were analyzed by detecting residual surface molecules by staining with a fluorochrome-labeled streptavidin antibody. Samples were handled in duplicates or triplicates. Measurements were performed with a BDFortessa.

BMDC generation/co-culture

BMDCs were generated as previously published (Boucheron et al., 2010). Briefly, BM was isolated from tibiae and femurs, and single-cell suspensions were cultured at 10×10^6 cells per 100 mm bacteriological Falcon petri dish in 10 ml complete T cell medium supplemented with 20 ng/ml GM-CSF (PeproTech). At day 3, an additional 10 ml complete T cell medium + 20 ng/ml GM-CSF was added. On days 6 and 9, half of the medium was removed, and cells were centrifuged and added with freshly prepared 10 ml complete T cell medium + 20 ng/ml GM-CSF. Non-adherent immature BMDCs were harvested on day 10 and stimulated with $OVA_{(323–339)}$ peptide (1 µg/ml) for 45 min at 37°C. Afterward, they were cultured at a 1:10 ratio with sorted naïve $CD4^+$ $OT\text{-}II^+$ T cells. On day 3, T cells were harvested and analyzed. For assessment of proliferation, T cells were labeled using Cell Proliferation Dye eFluor450 (Thermo Fisher Scientific) according to the manufacturer's protocol prior to the co-culture. To study the effect of CD28 blocking on proliferation, 40 µg/ml CTLA4-Ig was added to the culture.

Semiquantitative RT-PCR

Total RNA was isolated from total organs or from sorted $B220^+$ B cells, GC B cells, $CD4^+/CD8^+$ T cells, and Tfh from indicated

organs using RNeasy Mini Kit (Qiagen, Inc.). cDNA synthesis was performed using Superscript III First Strand Synthesis System (Invitrogen). Primers used are as follows: *Rinl* fw, 5′-AGACAGGGCTCCTCGGTGTA-3′; *Rinl* rev, 5′-CCAGCATCTCCC GTCTCTCT-3′; *Bcl6* fw, 5′-CTGCAGCGGCCTGTTCTACA-3′; *Bcl6* rev, 5′-AAGGTGCTGAGCGGGAGATG-3′ (Kitano et al., 2011); *Aicda* fw, 5′-CCAGGAACCGCTACTCGTTT-3′; and *Aicda* rev, 5′-GTCCGTCTCAGGCACTATG-3′.

IL-2 ELISA

IL-2 ELISA was performed using an ELISA MAX Deluxe Set Mouse IL-2 as described in the manufacturer's protocol (BioLegend). The O.D. was measured with an ELISA Reader (Multiscan GO, SkanIt Software for Microplate Readers RE) at 450 nM.

LCMV-specific IgG1 and IgG2c ELISA

For the measurement of LCMV-specific IgG1 antibodies, ELISA was performed as previously described with minor adaptations (Baumjohann et al., 2013). Briefly, 96-well Nunc MaxiSorp flat-bottom plates (Thermo Fisher Scientific) were coated with lysates of LCMV Armstrong-infected baby hamster kidney cells overnight. Nonspecific binding was blocked with PBS + 0.5% Tween 20 (Promega) + 10% FBS for 2 h at room temperature. Subsequently, serially diluted serum was added and incubated for another 2 h at room temperature. Rat anti-mouse IgG1 (Clone A85-1; BD Biosciences) or Rat anti-mouse IgG2c horseradish peroxidase (HRP; pooled anti-sera; SouthernBiotech) and ECL anti-rat IgG HRP linked whole antibody from goat (GE Healthcare UK Limited) were used to detect IgG1 antibodies upon the addition of TMB substrate (TMB substrate set; BioLegend). The O.D. was measured with an ELISA Reader (Multiscan GO, SkanIt Software for Microplate Readers RE) at 450 nM.

Bulk RNA-seq, sample preparation, and bioinformatic analysis

Total RNA was prepared from 1 to 2 × 10^6 sorted naïve ($CD25^-$ $CD44^{low}CD62^{high}$) or effector ($CD25^-$ $CD44^{high}CD62^{low}$) $CD4^+$ T cells using RNeasy Mini Kit (Qiagen, Inc.) as described in the manufacturer's protocol including an on-column digestion step (RNaseFree DNase Set; Qiagen, Inc.). The amount of total RNA was quantified using the Qubit 2.0 Fluorometric Quantitation system (Thermo Fisher Scientific), and the RNA integrity number was estimated using the Experion Automated Electrophoresis System (Bio-Rad). RNA-seq libraries were generated by the Biomedical Sequencing facility at the Center for Molecular Medicine using a Sciclone NGS Workstation (PerkinElmer) and a Zepyhr NGS Workstation (PerkinElmer) with the TruSeq Stranded mRNA LT sample preparation kit (Illumina). Library concentrations were determined with the Qubit 2.0 Fluorometric Quantitation system (Life Technologies) and were sequenced using the HiSeq 3000/4000 platform (Illumina) following the 50-bp single-read configuration. Following the raw data acquisition (HiSeq Control Software) and base calling (Real-Time Analysis Software, RTA, v2.7.7) that was performed on-instrument, the subsequent raw data processing involved programs based on Picard tools (https://broadinstitute.github.io/picard/) to generate sample-specific, unaligned BAM files. Sequence reads were subsequently mapped onto the mouse reference genome assembly build mm10 (a flavor of GRCm38) using Spliced Transcripts Alignment to a Reference (STAR) aligner (Dobin et al., 2013), which was run with options recommended by the ENCODE project. Aligned reads that overlapped Ensembl transcript features were counted with the Bioconductor (v3.12) GenomicAlignments (v1.26.0) package. Differential expression was tested using the Bioconductor DESeq2 package (v1.30.0; Love et al., 2014). The volcano plot was generated using GraphPad Prism and downstream analysis was performed using Ingenuity Pathway Analysis (Qiagen IPA).

Bioinformatics analysis of published RNA-seq data

RNA-seq from previously published data (Zhang et al., 2019) was downloaded from Immport (SDY998) as normalized $\log_2$-transformed data. Retrieved data was checked for quality and consistency after combining it with corresponding metadata. All data manipulation was performed in R (v4.1.2).

Statistical analysis

All statistical analyses were performed using GraphPadPrism software (v8.0.2). For single comparisons, paired or unpaired Student's *t* test or one-sample *T* test was performed as indicated in figure legends. For multiple comparisons, one-way or two-way ANOVA followed by Tukey's multiple-comparisons tests were performed. Horizontal lines indicate the mean, and error bars show the standard error of the mean (SEM).

Ethics statement

The animal study was reviewed and approved by the Austrian Federal Ministry for Education, Science and Art. Peripheral blood draws were performed from healthy human volunteers in accordance with the Ethics Committee of the Medical University of Vienna (EC number EK 1150/2015).

Online supplemental material

Fig. S1 shows how Rinl-KO mice were designed and generated, normal T cell development in the thymus of Rinl-KO mice, Rinl expression in various cell types, and distribution of immune cells in the spleen of WT and Rinl-KO mice in homeostasis. Fig. S2 shows how loss of Rinl affects immune cell homeostasis in older mice. Fig. S3 shows that Rinl does not regulate Th1, Th2, Th17, and Treg cell differentiation. Fig. S4 provides additional information about the analysis of splenocytes from WT and Rinl-KO mice after LCMV Armstrong infection. Fig. S5 shows how Rinl controls ICOS and IL-2 expression in effector $CD4^+$ T cells in vivo without affecting Tfr frequencies.

Data availability

The authors declare that the data supporting the findings of this research are available in the article and the supplemental material. The RNA-seq data generated during this study are available through Gene Expression Omnibus accession number GSE235805. The data underlying Fig. 10 G are openly available at Immport under SDY998.

Acknowledgments

We thank the Biomedical Sequencing Facility at the Center for Molecular Medicine for assistance with next-generation sequencing and Michael Schuster for initial data processing and analysis of RNA-seq data. Confocal immunofluorescence microscopy was carried out at Alembic, San Raffaele Scientific Institute and the Vita-Salute San Raffaele University. Mice were kept at the Core facility laboratory animal breeding and husbandry of the Medical University of Vienna. We also thank Dieter Printz of the FACS Core Unit at St. Anna Children's Cancer Research Institute for cell sorting and the National Institutes of Health Tetramer Facility for providing GP66-specific MHC class II tetramers. L Sandner would like to thank the European Federation of Immunology (EFIS) for awarding the EFIS-IL Short-term Fellowship.

This study has been funded by the Austrian Science Foundation through projects P19223 (R. Herbst), F7005, and doc.-funds (DOC) Programme 32 (W. Ellmeier), P27747 and P35436 (S. Sakaguchi), and P24265, P30885, and F7004 (all N. Boucheron). B. Woller was supported by the DOC-fFORTE Programme from the Austrian Academy of Sciences. L. Sandner received an EFIS-IL Short-term Fellowship for a research stay at Vita San Raffaele University and Division of Immunology, Transplantation and Infectious Diseases, IRCCS San Raffaele Scientific Institute, Milan, Italy. M. Kuka has been supported by the Italian Ministry of University and Research grants PRIN-2017ZXT5WR and PRIN-20209Y5YFZ.

Author contributions: Conceptualization: L. Sandner, W. Ellmeier, R. Herbst, and N. Boucheron. Methodology: L. Sandner, A. Schebesta, S. Sakaguchi, E. Sala, M. Kuka, T. Frey, K. Schmetterer, B. Woller, and I. Taniuchi. Investigation: L. Sandner, N. Boucheron, M. Alteneder, C. Zhu, R. Rica, M. Khan, P. Hoffmann, A. Schebesta, S. Sakaguchi, M. Madern, A. Tosevska, M. Bonelli, B. Woller, I. Taniuchi, E. Sala, M. Kuka, T. Frey, K. Schmetterer, and R. Herbst. Visualization: L. Sandner, A. Schebesta, and A. Tosevska. Funding acquisition: N. Boucheron, R. Herbst, S. Sakaguchi, L. Sandner, B. Woller, and W. Ellmeier. Project administration: L. Sandner and N. Boucheron. Supervision: N. Boucheron. Writing—original draft: L. Sandner, N. Boucheron, S. Sakaguchi, and W. Ellmeier. Writing—review & editing: L. Sandner, M. Alteneder, R. Rica, B. Woller, E. Sala, T. Frey, A. Tosevska, M. Madern, M. Bonelli, M. Khan, M. Iannacone, M. Kuka, W. Ellmeier, S. Sakaguchi, R. Herbst, N. Boucheron. L. Sandner, W. Ellmeier, R. Herbst, and N. Boucheron designed the research; L. Sandner performed most of the experiments and analyzed the data. M. Alteneder, C. Zhu, R. Rica, and P. Hoffmann contributed to in vivo experiments; A. Schebesta performed semiquantitative PCR analysis; S. Sakaguchi contributed to LCMV infection experiments and analyzed data. L. Sandner, M. Madern, A. Tosevska, and M. Bonelli performed bioinformatics analysis; B. Woller, W. Ellmeier, R. Herbst, and I. Taniuchi generated the Rinl-KO mice; E. Sala, M. Kuka, and M. Iannacone performed confocal microscopy experiments; T. Frey and K. Schmetterer performed CRISPR-Cas9 mediated deletion in human $CD4^+$ T cells; M. Kuka contributed to revision experiments; L. Sandner and N. Boucheron wrote the manuscript with contributions from all co-authors.

Disclosures: M. Iannacone consults or sits on advisory boards for the following companies: Asher Biotherapeutics, San Carlos, CA; GentiBio, Cambridge, MA; Clexio Biosciences, Petach Tikva, Israel; Sybilla Biotech, Trento, Italy; BlueJay Therapeutics, San Mateo, CA; Bristol Myers Squibb, New York, NY; and Aligos Therapeutics, South San Francisco, CA. No other disclosures were reported.

Submitted: 25 August 2022
Revised: 7 June 2023
Accepted: 21 August 2023

References

Agola, J.O., P.A. Jim, H.H. Ward, S. Basuray, and A. Wandinger-Ness. 2011. Rab GTPases as regulators of endocytosis, targets of disease and therapeutic opportunities. *Clin. Genet.* 80:305–318. https://doi.org/10.1111/j.1399-0004.2011.01724.x

Badour, K., M.K.H. McGavin, J. Zhang, S. Freeman, C. Vieira, D. Filipp, M. Julius, G.B. Mills, and K.A. Siminovitch. 2007. Interaction of the Wiskott-Aldrich syndrome protein with sorting nexin 9 is required for CD28 endocytosis and cosignaling in T cells. *Proc. Natl. Acad. Sci. USA.* 104:1593–1598. https://doi.org/10.1073/pnas.0610543104

Baumjohann, D., R. Kageyama, J.M. Clingan, M.M. Morar, S. Patel, D. de Kouchkovsky, O. Bannard, J.A. Bluestone, M. Matloubian, K.M. Ansel, and L.T. Jeker. 2013. The microRNA cluster miR-17~92 promotes TFH cell differentiation and represses subset-inappropriate gene expression. *Nat. Immunol.* 14:840–848. https://doi.org/10.1038/ni.2642

Bos, J.L., H. Rehmann, and A. Wittinghofer. 2007. GEFs and GAPs: Critical elements in the control of small G proteins. *Cell.* 129:865–877. https://doi.org/10.1016/j.cell.2007.05.018

Boucheron, N., O. Sharif, A. Schebesta, A. Croxford, J. Raberger, U. Schmidt, B. Vigl, J. Bauer, R. Bankoti, H. Lassmann, et al. 2010. The protein tyrosine kinase Tec regulates a CD44highCD62L- Th17 subset. *J. Immunol.* 185:5111–5119. https://doi.org/10.4049/jimmunol.1001734

Carney, D.S., B.A. Davies, and B.F. Horazdovsky. 2006. Vps9 domain-containing proteins: Activators of Rab5 GTPases from yeast to neurons. *Trends Cell Biol.* 16:27–35. https://doi.org/10.1016/j.tcb.2005.11.001

Céfaï, D., H. Schneider, O. Matangkasombut, H. Kang, J. Brody, and C.E. Rudd. 1998. CD28 receptor endocytosis is targeted by mutations that disrupt phosphatidylinositol 3-kinase binding and costimulation. *J. Immunol.* 160:2223–2230. https://doi.org/10.4049/jimmunol.160.5.2223

Choi, Y.S., R. Kageyama, D. Eto, T.C. Escobar, R.J. Johnston, L. Monticelli, C. Lao, and S. Crotty. 2011. ICOS receptor instructs T follicular helper cell versus effector cell differentiation via induction of the transcriptional repressor Bcl6. *Immunity.* 34:932–946. https://doi.org/10.1016/j.immuni.2011.03.023

Ciraci, C., J.R. Janczy, N. Jain, S. Haasken, C. Pecli E Silva, C.F. Benjamim, J.J. Sadler, A.K. Olivier, Y. Iwakura, D.M. Shayakhmetov, et al. 2016. Immune complexes indirectly suppress the generation of Th17 responses in vivo. *PLoS One.* 11:e0151252. https://doi.org/10.1371/journal.pone.0151252

Crotty, S. 2011. Follicular helper CD4 T cells (TFH). *Annu. Rev. Immunol.* 29:621–663. https://doi.org/10.1146/annurev-immunol-031210-101400

de Leval, L., D.S. Rickman, C. Thielen, A.d. Reynies, Y.L. Huang, G. Delsol, L. Lamant, K. Leroy, J. Brière, T. Molina, et al. 2007. The gene expression profile of nodal peripheral T-cell lymphoma demonstrates a molecular link between angioimmunoblastic T-cell lymphoma (AITL) and follicular helper T (TFH) cells. *Blood.* 109:4952–4963. https://doi.org/10.1182/blood-2006-10-055145

Deininger, K., M. Eder, E.R. Kramer, W. Zieglgänsberger, H.U. Dodt, K. Dornmair, J. Colicelli, and R. Klein. 2008. The Rab5 guanylate exchange factor Rin1 regulates endocytosis of the EphA4 receptor in mature excitatory neurons. *Proc. Natl. Acad. Sci. USA.* 105:12539–12544. https://doi.org/10.1073/pnas.0801174105

Di Bartolo, V., B. Montagne, M. Salek, B. Jungwirth, F. Carrette, J. Fourtane, N. Sol-Foulon, F. Michel, O. Schwartz, W.D. Lehmann, and O. Acuto. 2007. A novel pathway down-modulating T cell activation involves HPK-1-dependent recruitment of 14-3-3 proteins on SLP-76. *J. Exp. Med.* 204:681–691. https://doi.org/10.1084/jem.20062066

DiToro, D., C.J. Winstead, D. Pham, S. Witte, R. Andargachew, J.R. Singer, C.G. Wilson, C.L. Zindl, R.J. Luther, D.J. Silberger, et al. 2018. Differential IL-2 expression defines developmental fates of follicular versus non-follicular helper T cells. *Science*. 361:eaao2933. https://doi.org/10.1126/science.aao2933

Dobin, A., C.A. Davis, F. Schlesinger, J. Drenkow, C. Zaleski, S. Jha, P. Batut, M. Chaisson, and T.R. Gingeras. 2013. STAR: Ultrafast universal RNA-seq aligner. *Bioinformatics*. 29:15–21. https://doi.org/10.1093/bioinformatics/bts635

Fagerberg, L., B.M. Hallström, P. Oksvold, C. Kampf, D. Djureinovic, J. Odeberg, M. Habuka, S. Tahmasebpoor, A. Danielsson, K. Edlund, et al. 2014. Analysis of the human tissue-specific expression by genome-wide integration of transcriptomics and antibody-based proteomics. *Mol. Cell. Proteomics*. 13:397–406. https://doi.org/10.1074/mcp.M113.035600

Fazilleau, N., L.J. McHeyzer-Williams, H. Rosen, and M.G. McHeyzer-Williams. 2009. The function of follicular helper T cells is regulated by the strength of T cell antigen receptor binding. *Nat. Immunol.* 10:375–384. https://doi.org/10.1038/ni.1704

Ferguson, S.E., S. Han, G. Kelsoe, and C.B. Thompson. 1996. CD28 is required for germinal center formation. *J. Immunol.* 156:4576–4581. https://doi.org/10.4049/jimmunol.156.12.4576

Finetti, F., L. Patrussi, G. Masi, A. Onnis, D. Galgano, O.M. Lucherini, G.J. Pazour, and C.T. Baldari. 2014. Specific recycling receptors are targeted to the immune synapse by the intraflagellar transport system. *J. Cell Sci.* 127:1924–1937. https://doi.org/10.1242/jcs.139337

Gong, F., Q. Su, D. Jiang, J. Chen, Y. Pan, and X. Huang. 2014. High frequency of circulating follicular helper T cells in patients with bronchial asthma. *Clin. Lab.* 60:963–968. https://doi.org/10.7754/Clin.Lab.2013.130427

Hale, J.S., B. Youngblood, D.R. Latner, A.U.R. Mohammed, L. Ye, R.S. Akondy, T. Wu, S.S. Iyer, and R. Ahmed. 2013. Distinct memory CD4$^+$ T cells with commitment to T follicular helper- and T helper 1-cell lineages are generated after acute viral infection. *Immunity*. 38:805–817. https://doi.org/10.1016/j.immuni.2013.02.020

Hama, H., G.G. Tall, and B.F. Horazdovsky. 1999. Vps9p is a guanine nucleotide exchange factor involved in vesicle-mediated vacuolar protein transport. *J. Biol. Chem.* 274:15284–15291. https://doi.org/10.1074/jbc.274.21.15284

Jogdand, G.M., S. Mohanty, and S. Devadas. 2016. Regulators of Tfh cell differentiation. *Front. Immunol.* 7:520. https://doi.org/10.3389/fimmu.2016.00520

Johnston, R.J., A.C. Poholek, D. DiToro, I. Yusuf, D. Eto, B. Barnett, A.L. Dent, J. Craft, and S. Crotty. 2009. Bcl6 and Blimp-1 are reciprocal and antagonistic regulators of T follicular helper cell differentiation. *Science*. 325:1006–1010. https://doi.org/10.1126/science.1175870

Jones, L., W.Q. Ho, S. Ying, L. Ramakrishna, K.G. Srinivasan, M. Yurieva, W.P. Ng, S. Subramaniam, N.H. Hamadee, S. Joseph, et al. 2016. A subpopulation of high IL-21-producing CD4(+) T cells in Peyer's Patches is induced by the microbiota and regulates germinal centers. *Sci. Rep.* 6:30784. https://doi.org/10.1038/srep30784

Kajiho, H., S. Fukushima, K. Kontani, and T. Katada. 2012. RINL, guanine nucleotide exchange factor Rab5-subfamily, is involved in the EphA8-degradation pathway with odin. *PLoS One*. 7:e30575. https://doi.org/10.1371/journal.pone.0030575

Kajiho, H., K. Saito, K. Tsujita, K. Kontani, Y. Araki, H. Kurosu, and T. Katada. 2003. RIN3: A novel Rab5 GEF interacting with amphiphysin II involved in the early endocytic pathway. *J. Cell Sci.* 116:4159–4168. https://doi.org/10.1242/jcs.00718

Kaneko, N., H.H. Kuo, J. Boucau, J.R. Farmer, H. Allard-Chamard, V.S. Mahajan, A. Piechocka-Trocha, K. Lefteri, M. Osborn, J. Bals, et al. 2020. Loss of Bcl-6-expressing T follicular helper cells and germinal centers in COVID-19. *Cell*. 183:143–157.e13. https://doi.org/10.1016/j.cell.2020.08.025

Kim, C.H., L.S. Rott, I. Clark-Lewis, D.J. Campbell, L. Wu, and E.C. Butcher. 2001. Subspecialization of CXCR5+ T cells: B helper activity is focused in a germinal center-localized subset of CXCR5+ T cells. *J. Exp. Med.* 193:1373–1381. https://doi.org/10.1084/jem.193.12.1373

Kitano, M., S. Moriyama, Y. Ando, M. Hikida, Y. Mori, T. Kurosaki, and T. Okada. 2011. Bcl6 protein expression shapes pre-germinal center B cell dynamics and follicular helper T cell heterogeneity. *Immunity*. 34:961–972. https://doi.org/10.1016/j.immuni.2011.03.025

Lane, P., C. Burdet, S. Hubele, D. Scheidegger, U. Müller, F. McConnell, and M. Kosco-Vilbois. 1994. B cell function in mice transgenic for mCTLA4-H gamma 1: Lack of germinal centers correlated with poor affinity maturation and class switching despite normal priming of CD4$^+$ T cells. *J. Exp. Med.* 179:819–830. https://doi.org/10.1084/jem.179.3.819

Linterman, M.A., A.E. Denton, D.P. Divekar, I. Zvetkova, L. Kane, C. Ferreira, M. Veldhoen, S. Clare, G. Dougan, M. Espéli, and K.G.C. Smith. 2014. CD28 expression is required after T cell priming for helper T cell responses and protective immunity to infection. *Elife*. 3:e03180. https://doi.org/10.7554/eLife.03180

Locci, M., J.E. Wu, F. Arumemi, Z. Mikulski, C. Dahlberg, A.T. Miller, and S. Crotty. 2016. Activin A programs the differentiation of human TFH cells. *Nat. Immunol.* 17:976–984. https://doi.org/10.1038/ni.3494

Love, M.I., W. Huber, and S. Anders. 2014. Moderated estimation of fold change and dispersion for RNA-seq data with DESeq2. *Genome Biol.* 15:550. https://doi.org/10.1186/s13059-014-0550-8

Ma, J., C. Zhu, B. Ma, J. Tian, S.E. Baidoo, C. Mao, W. Wu, J. Chen, J. Tong, M. Yang, et al. 2012. Increased frequency of circulating follicular helper T cells in patients with rheumatoid arthritis. *Clin. Dev. Immunol.* 2012:827480. https://doi.org/10.1155/2012/827480

Marshall, H.D., A. Chandele, Y.W. Jung, H. Meng, A.C. Poholek, I.A. Parish, R. Rutishauser, W. Cui, S.H. Kleinstein, J. Craft, and S.M. Kaech. 2011. Differential expression of Ly6C and T-bet distinguish effector and memory Th1 CD4(+) cell properties during viral infection. *Immunity*. 35:633–646. https://doi.org/10.1016/j.immuni.2011.08.016

McAdam, A.J., T.T. Chang, A.E. Lumelsky, E.A. Greenfield, V.A. Boussiotis, J.S. Duke-Cohan, T. Chernova, N. Malenkovich, C. Jabs, V.K. Kuchroo, et al. 2000. Mouse inducible costimulatory molecule (ICOS) expression is enhanced by CD28 costimulation and regulates differentiation of CD4$^+$ T cells. *J. Immunol.* 165:5035–5040. https://doi.org/10.4049/jimmunol.165.9.5035

Nurieva, R.I., Y. Chung, G.J. Martinez, X.O. Yang, S. Tanaka, T.D. Matskevitch, Y.H. Wang, and C. Dong. 2009. Bcl6 mediates the development of T follicular helper cells. *Science*. 325:1001–1005. https://doi.org/10.1126/science.1176676

Pfeffer, S.R. 2013. Rab GTPase regulation of membrane identity. *Curr. Opin. Cell Biol.* 25:414–419. https://doi.org/10.1016/j.ceb.2013.04.002

Preite, S., B. Huang, J.L. Cannons, D.B. McGavern, and P.L. Schwartzberg. 2019. PI3K orchestrates T follicular helper cell differentiation in a context dependent manner: Implications for autoimmunity. *Front. Immunol.* 9:3079. https://doi.org/10.3389/fimmu.2018.03079

Rasheed, A.U., H.P. Rahn, F. Sallusto, M. Lipp, and G. Müller. 2006. Follicular B helper T cell activity is confined to CXCR5(hi)ICOS(hi) CD4 T cells and is independent of CD57 expression. *Eur. J. Immunol.* 36:1892–1903. https://doi.org/10.1002/eji.200636136

Raychaudhuri, S., B.P. Thomson, E.F. Remmers, S. Eyre, A. Hinks, C. Guiducci, J.J. Catanese, G. Xie, E.A. Stahl, R. Chen, et al. 2009. Genetic variants at CD28, PRDM1 and CD2/CD58 are associated with rheumatoid arthritis risk. *Nat. Genet.* 41:1313–1318. https://doi.org/10.1038/ng.479

Rohr, J., S. Guo, J. Huo, A. Bouska, C. Lachel, Y. Li, P.D. Simone, W. Zhang, Q. Gong, C. Wang, et al. 2016. Recurrent activating mutations of CD28 in peripheral T-cell lymphomas. *Leukemia*. 30:1062–1070. https://doi.org/10.1038/leu.2015.357

Roncador, G., J.F. García Verdes-Montenegro, S. Tedoldi, J.C. Paterson, W. Klapper, E. Ballabio, L. Maestre, S. Pileri, M.L. Hansmann, M.A. Piris, et al. 2007. Expression of two markers of germinal center T cells (SAP and PD-1) in angioimmunoblastic T-cell lymphoma. *Haematologica*. 92:1059–1066. https://doi.org/10.3324/haematol.10864

Saito, K., J. Murai, H. Kajiho, K. Kontani, H. Kurosu, and T. Katada. 2002. A novel binding protein composed of homophilic tetramer exhibits unique properties for the small GTPase Rab5. *J. Biol. Chem.* 277:3412–3418. https://doi.org/10.1074/jbc.M106276200

Schaerli, P., K. Willimann, A.B. Lang, M. Lipp, P. Loetscher, and B. Moser. 2000. CXC chemokine receptor 5 expression defines follicular homing T cells with B cell helper function. *J. Exp. Med.* 192:1553–1562. https://doi.org/10.1084/jem.192.11.1553

Seki, A., and S. Rutz. 2018. Optimized RNP transfection for highly efficient CRISPR/Cas9-mediated gene knockout in primary T cells. *J. Exp. Med.* 215:985–997. https://doi.org/10.1084/jem.20171626

Shahinian, A., K. Pfeffer, K.P. Lee, T.M. Kündig, K. Kishihara, A. Wakeham, K. Kawai, P.S. Ohashi, C.B. Thompson, and T.W. Mak. 1993. Differential T cell costimulatory requirements in CD28-deficient mice. *Science*. 261:609–612. https://doi.org/10.1126/science.7688139

Simanshu, D.K., D.V. Nissley, and F. McCormick. 2017. RAS proteins and their regulators in human disease. *Cell*. 170:17–33. https://doi.org/10.1016/j.cell.2017.06.009

Stenmark, H. 2009. Rab GTPases as coordinators of vesicle traffic. *Nat. Rev. Mol. Cell Biol.* 10:513–525. https://doi.org/10.1038/nrm2728

Suto, A., D. Kashiwakuma, S.i. Kagami, K. Hirose, N. Watanabe, K. Yokote, Y. Saito, T. Nakayama, M.J. Grusby, I. Iwamoto, and H. Nakajima. 2008. Development and characterization of IL-21-producing CD4+ T cells. *J. Exp. Med.* 205:1369–1379. https://doi.org/10.1084/jem.20072057

Tall, G.G., M.A. Barbieri, P.D. Stahl, and B.F. Horazdovsky. 2001. Ras-activated endocytosis is mediated by the Rab5 guanine nucleotide exchange activity of RIN1. *Dev. Cell.* 1:73–82. https://doi.org/10.1016/S1534-5807(01)00008-9

Tangye, S.G., C.S. Ma, R. Brink, and E.K. Deenick. 2013. The good, the bad and the ugly: TFH cells in human health and disease. *Nat. Rev. Immunol.* 13:412–426. https://doi.org/10.1038/nri3447

Thompson, C.B., T. Lindsten, J.A. Ledbetter, S.L. Kunkel, H.A. Young, S.G. Emerson, J.M. Leiden, and C.H. June. 1989. CD28 activation pathway regulates the production of multiple T-cell-derived lymphokines/cytokines. *Proc. Natl. Acad. Sci. USA.* 86:1333–1337. https://doi.org/10.1073/pnas.86.4.1333

Tubo, N.J., A.J. Pagán, J.J. Taylor, R.W. Nelson, J.L. Linehan, J.M. Ertelt, E.S. Huseby, S.S. Way, and M.K. Jenkins. 2013. Single naive CD4+ T cells from a diverse repertoire produce different effector cell types during infection. *Cell.* 153:785–796. https://doi.org/10.1016/j.cell.2013.04.007

Vogelzang, A., H.M. McGuire, D. Yu, J. Sprent, C.R. Mackay, and C. King. 2008. A fundamental role for interleukin-21 in the generation of T follicular helper cells. *Immunity.* 29:127–137. https://doi.org/10.1016/j.immuni.2008.06.001

Walker, L.S., A. Gulbranson-Judge, S. Flynn, T. Brocker, C. Raykundalia, M. Goodall, R. Förster, M. Lipp, and P. Lane. 1999. Compromised OX40 function in CD28-deficient mice is linked with failure to develop CXC chemokine receptor 5-positive CD4 cells and germinal centers. *J. Exp. Med.* 190:1115–1122. https://doi.org/10.1084/jem.190.8.1115

Wan, S., L. Ni, X. Zhao, X. Liu, W. Xu, W. Jin, X. Wang, and C. Dong. 2021. Costimulation molecules differentially regulate the ERK-Zfp831 axis to shape T follicular helper cell differentiation. *Immunity.* 54:2740–2755.e6. https://doi.org/10.1016/j.immuni.2021.09.018

Wang, C.J., F. Heuts, V. Ovcinnikovs, L. Wardzinski, C. Bowers, E.M. Schmidt, A. Kogimtzis, R. Kenefeck, D.M. Sansom, and L.S.K. Walker. 2015. CTLA-4 controls follicular helper T-cell differentiation by regulating the strength of CD28 engagement. *Proc. Natl. Acad. Sci. USA.* 112:524–529. https://doi.org/10.1073/pnas.1414576112

Weber, J.P., F. Fuhrmann, R.K. Feist, A. Lahmann, M.S. Al Baz, L.J. Gentz, D. Vu Van, H.W. Mages, C. Haftmann, R. Riedel, et al. 2015. ICOS maintains the T follicular helper cell phenotype by down-regulating Krüppel-like factor 2. *J. Exp. Med.* 212:217–233. https://doi.org/10.1084/jem.20141432

Woller, B., S. Luiskandl, M. Popovic, B.E.M. Prieler, G. Ikonge, M. Mutzl, H. Rehmann, and R. Herbst. 2011. Rin-like, a novel regulator of endocytosis, acts as guanine nucleotide exchange factor for Rab5a and Rab22. *Biochim. Biophys. Acta.* 1813:1198–1210. https://doi.org/10.1016/j.bbamcr.2011.03.005

Xu, L., Y. Cao, Z. Xie, Q. Huang, Q. Bai, X. Yang, R. He, Y. Hao, H. Wang, T. Zhao, et al. 2015. The transcription factor TCF-1 initiates the differentiation of T(FH) cells during acute viral infection. *Nat. Immunol.* 16:991–999. https://doi.org/10.1038/ni.3229

Yang, X., and K.T. Hayglass. 1993. Allergen-dependent induction of interleukin-4 synthesis in vivo. *Immunology.* 78:74–79.

Yu, D., S. Rao, L.M. Tsai, S.K. Lee, Y. He, E.L. Sutcliffe, M. Srivastava, M. Linterman, L. Zheng, N. Simpson, et al. 2009. The transcriptional repressor Bcl-6 directs T follicular helper cell lineage commitment. *Immunity.* 31:457–468. https://doi.org/10.1016/j.immuni.2009.07.002

Yue, F., Y. Cheng, A. Breschi, J. Vierstra, W. Wu, T. Ryba, R. Sandstrom, Z. Ma, C. Davis, B.D. Pope, et al. 2014. A comparative encyclopedia of DNA elements in the mouse genome. *Nature.* 515:355–364. https://doi.org/10.1038/nature13992

Zhang, F., K. Wei, K. Slowikowski, C.Y. Fonseka, D.A. Rao, S. Kelly, S.M. Goodman, D. Tabechian, L.B. Hughes, K. Salomon-Escoto, et al. 2019. Defining inflammatory cell states in rheumatoid arthritis joint synovial tissues by integrating single-cell transcriptomics and mass cytometry. *Nat. Immunol.* 20:928–942. https://doi.org/10.1038/s41590-019-0378-1

JEM

Supplemental material

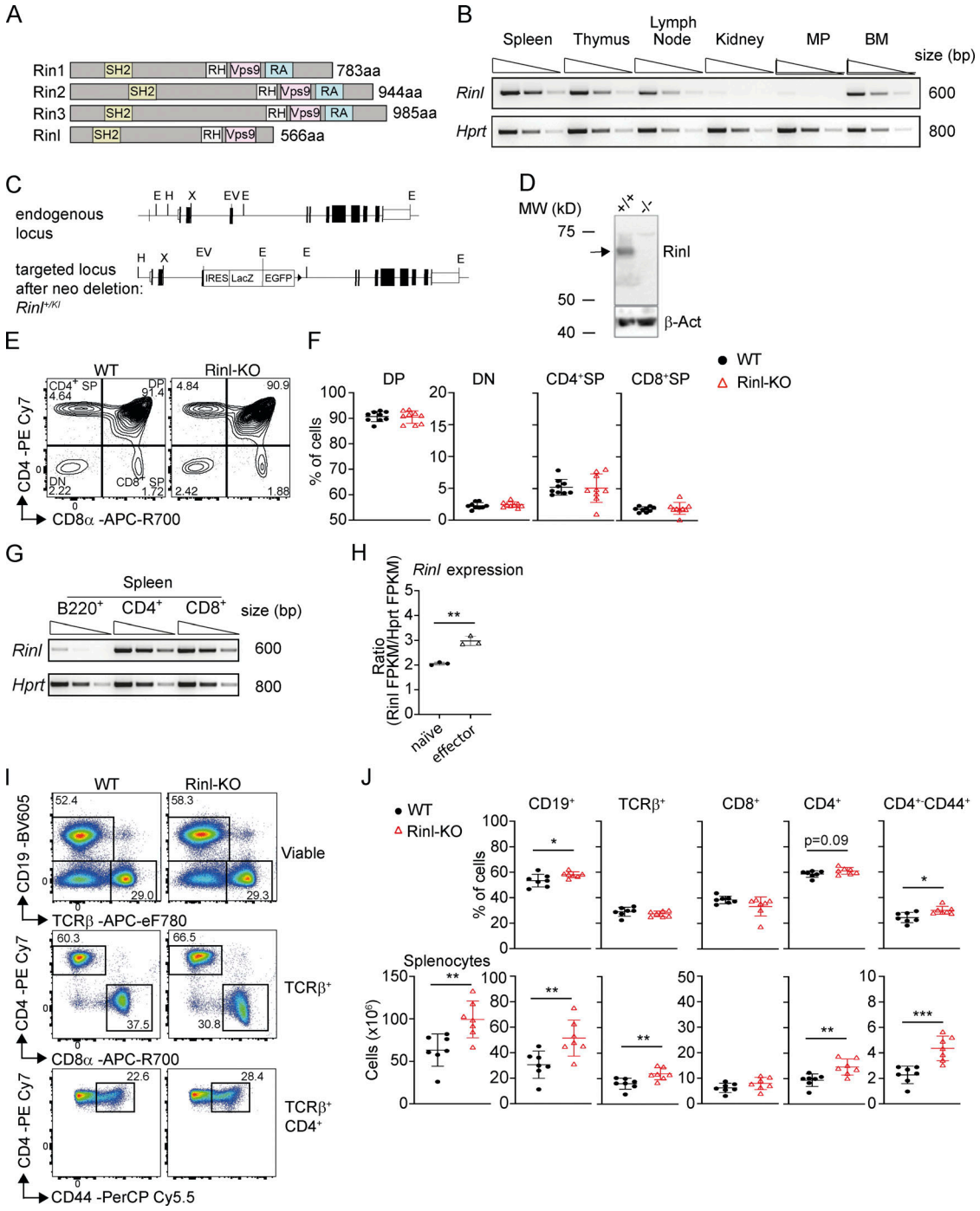

Figure S1. **Rinl is highly expressed in lymphoid organs and impacts T cell homeostasis in the spleen. (A)** Schematic representation of Ras interaction/interference (Rin) family members Rin1-Rin3 and Rinl. **(B)** Semiquantitative PCR of *Rinl* expression in different organs of WT mice. *Hprt* expression was used as control. **(C)** Rinl locus before and after targeting. *Rinl* has 12 exons (depicted as filled black boxes) and exons 1–11 encode for Rinl protein. Introns are represented by connecting lines. A STOP codon in the reading frame of exon 4 followed by IRES-LacZ::GFP cassette and a floxed neomycin was used to inactivate *Rinl*. Rinl^{+}/KI mice were generated by crossing Rinl^{+}/KI-neo mice with CMV-Cre mice to delete neomycin. **(D)** Immunoblot analysis depicting Rinl expression in thymocytes of the indicated genotype. The arrow indicates the position of Rinl at 60 kD. β-Actin protein abundance was used to confirm equal loading. **(E)** Representative contour plots of thymocyte gating. **(F)** Summary graphs show the percentages of double positive (DP), double negative (DN), single positive (SP) CD4^{+}, and SP CD8^{+} thymocytes. **(G)** Semiquantitative PCR of *Rinl* expression in B220^{+}, CD4^{+}, and CD8^{+} cells of WT spleens. **(H)** *Rinl* expression level among naïve (CD62L^{+}CD44^{-}) and effector (CD62L^{-}CD44^{+}) CD4^{+} T cells. Data are expressed as fragments per kilobase of transcript per million fragments mapped (FPKM) and Rinl expression was normalized to Hprt expression. **(I)** Representative pseudocolor plots for gating of CD19^{+}, TCRβ^{+}, CD4^{+}, CD8^{+}, and CD4^{+}CD44^{+} cells from the spleen. **(J)** Quantification (upper panel) and summary of cell numbers (lower panel) of I. The summary of nine (F) or seven (J) mice per genotype analyzed in three independent experiments is shown. Mean ± SEM are shown along individual data points in the graphs. Data were statistically analyzed using unpaired two-tailed *t* tests. *P < 0.05, **P < 0.01, ***P < 0.001. Aa, amino acid; SH, Src-homology; Vps, Vacuolar protein sorting-associated protein; E, EcoRI; X, XhoI; V; EcoR; H, HindII. Source data are available for this figure: SourceData FS1.

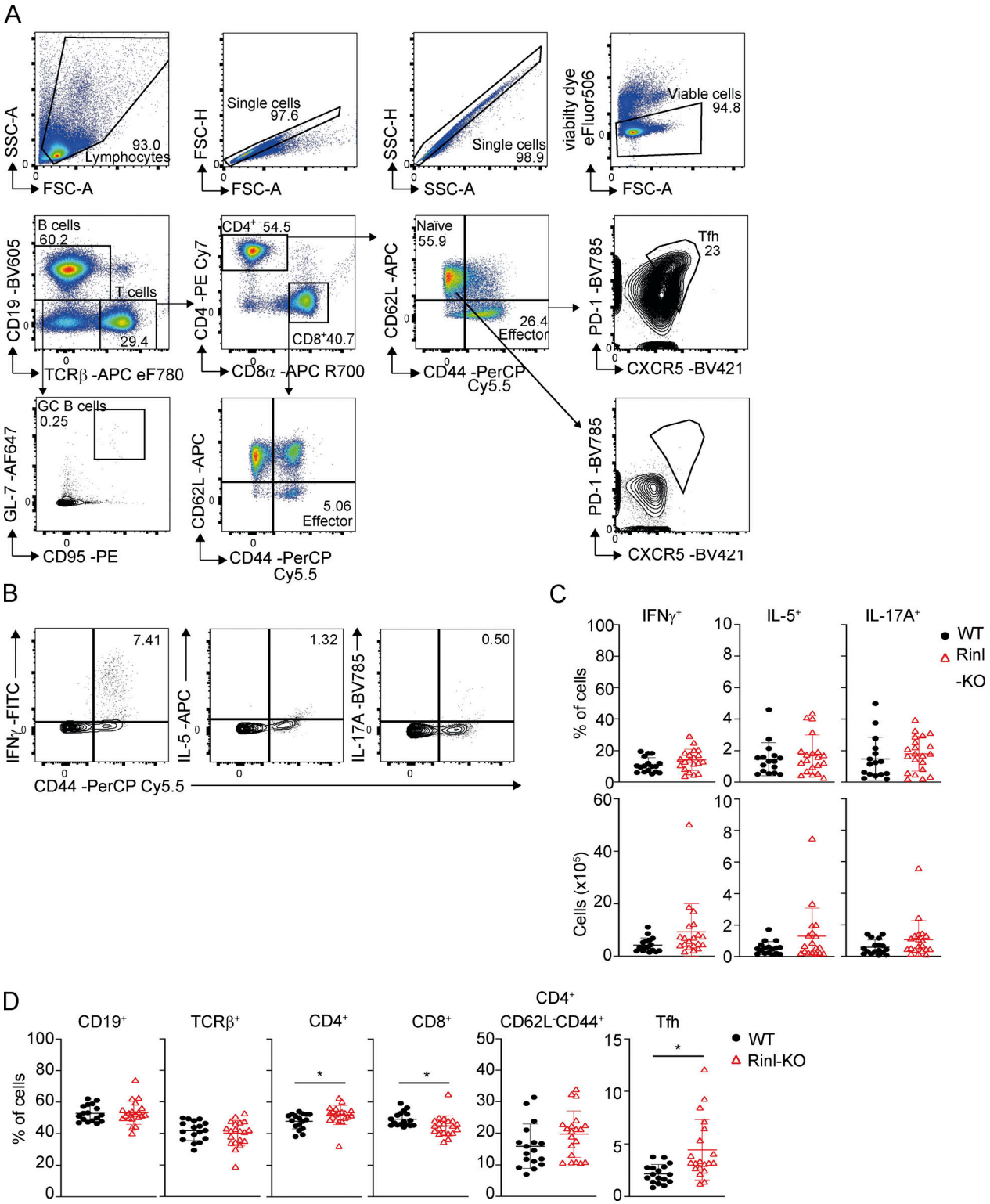

Figure S2. **Loss of Rinl affects peripheral T cell homeostasis in older mice. (A)** Gating strategy for analysis of lymphocyte subsets in the spleen of older WT and Rinl-KO mice. **(B)** Representative gating of cytokine producing CD4+ T cells of spleens of older mice **(C)** Summary graphs of cytokine-producing cells. **(D)** Summary graphs of cell subsets in peripheral LNs of older WT and Rinl-KO mice. Summary of 16–20 mice that were analyzed in three independent experiments are shown (C and D). Mean ± SEM are shown along individual data points in the graphs. Data were statistically analyzed using unpaired two-tailed *t* tests. *P < 0.05.

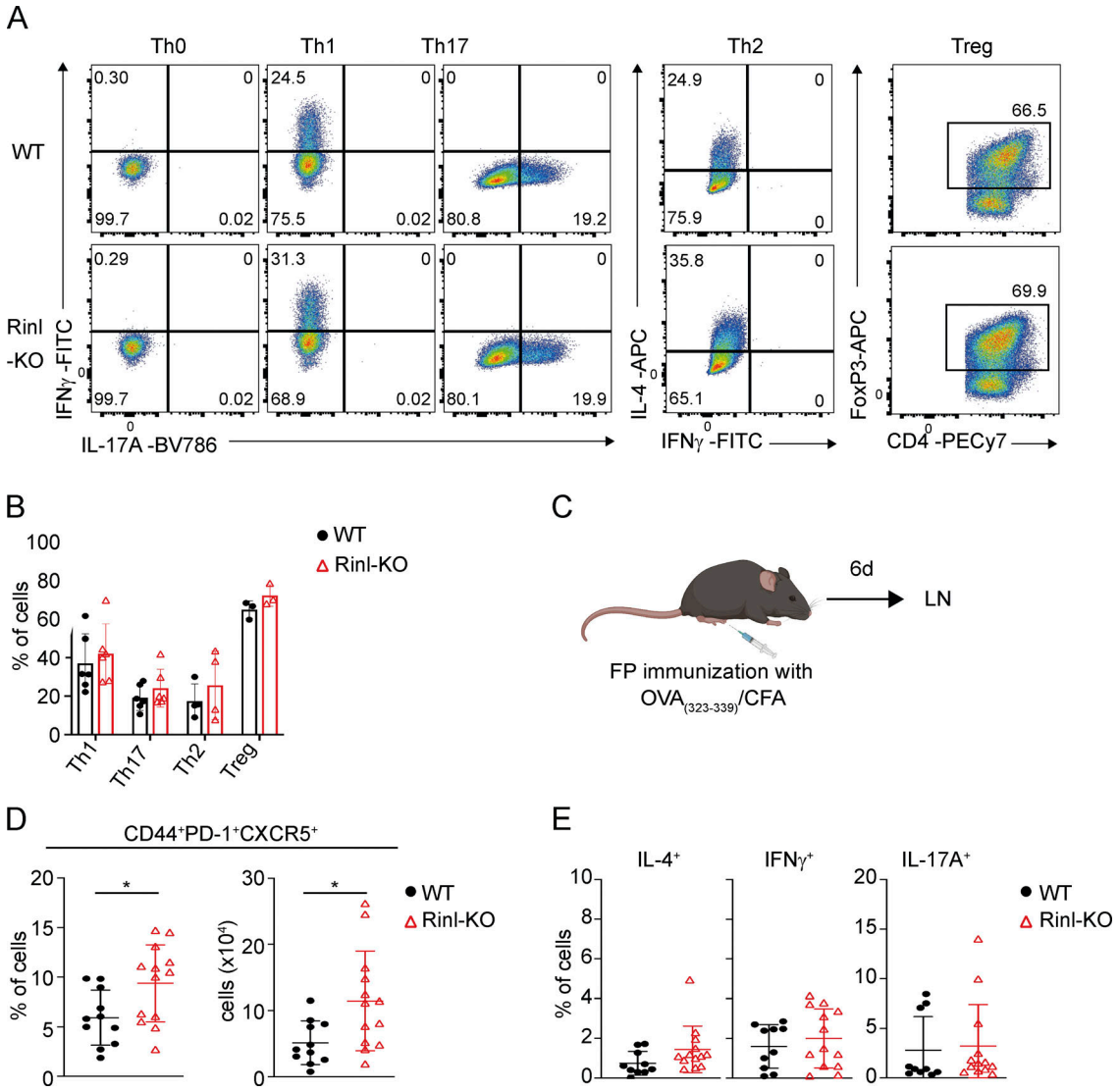

Figure S3. **Rinl does not regulate Th cell differentiation in vitro and in vivo. (A)** Representative contour plots of cytokine-producing CD4⁺ T cells after in vitro differentiation under Th1, Th2, Th17, or Treg skewing conditions. **(B)** Summary of A. **(C)** Experimental scheme. **(D)** Summary graphs of frequencies and cell numbers of Tfh. **(E)** Summary graphs of cytokine-producing cells. Data show summary of 3–6 (B) and 9–13 (D and E) mice analyzed in three to four independent experiments. Mean ± SEM are shown along individual data points in the graphs. Data were statistically analyzed using paired two-tailed *t* tests. *P < 0.05.

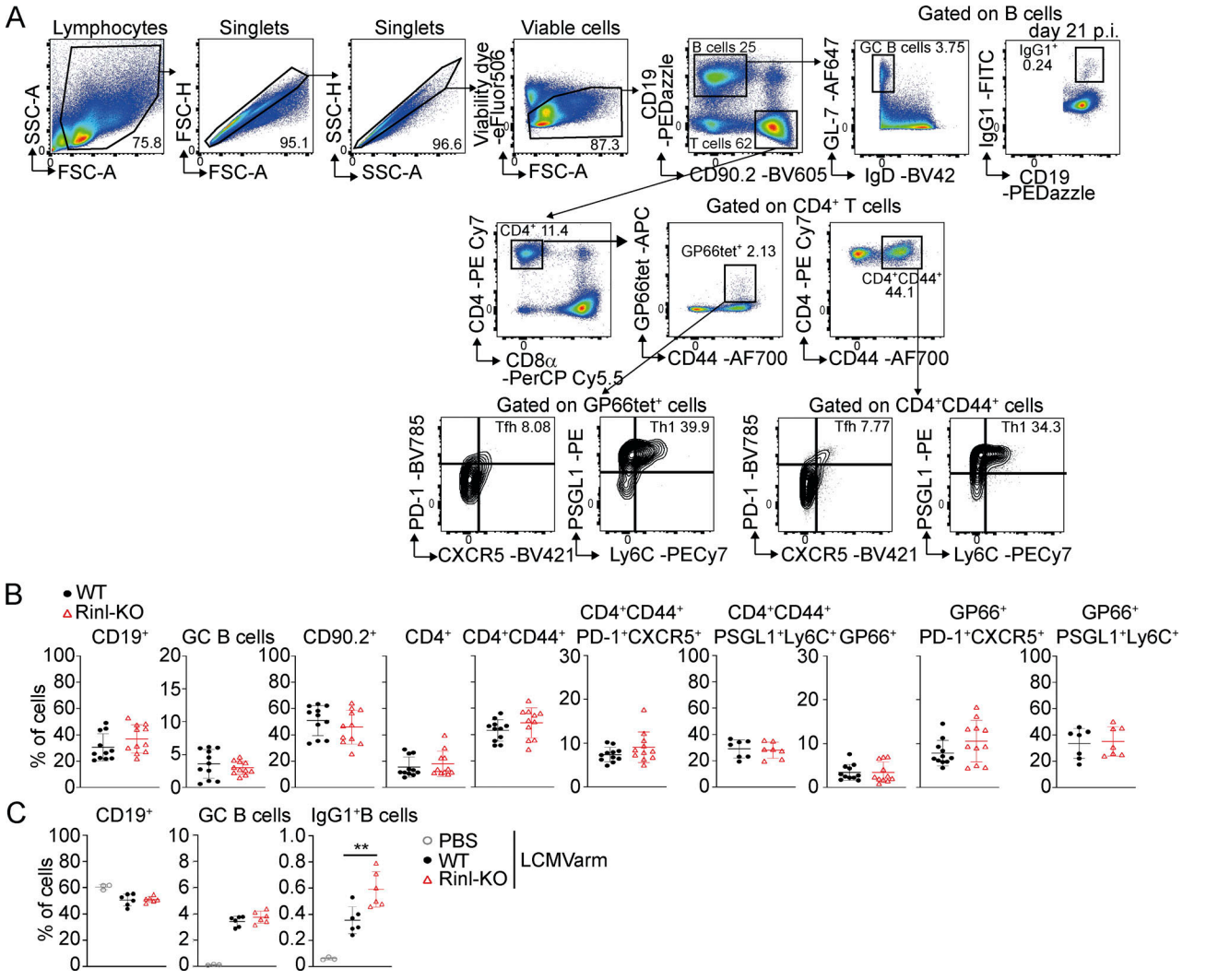

Figure S4. **Analysis of spleens from WT and Rinl-KO mice after LCMV Armstrong infection. (A)** Gating strategy of spleen of WT and Rinl-KO mice after LCMV infection **(B)**. Summary diagrams depict frequencies of lymphocyte subsets from spleens from WT and Rinl-KO mice 8 dpi. **(C)** Summary diagrams depict frequencies of B cell subsets from spleens from WT and Rinl-KO mice 21 dpi. Data show a summary of 11 (B) or 6 (C) mice per group analyzed in 3 (B) or 2 (C) independent experiments. Mean ± SEM are shown along individual data points in the graphs. Data were statistically analyzed using unpaired two-tailed *t* tests. **P < 0.01.

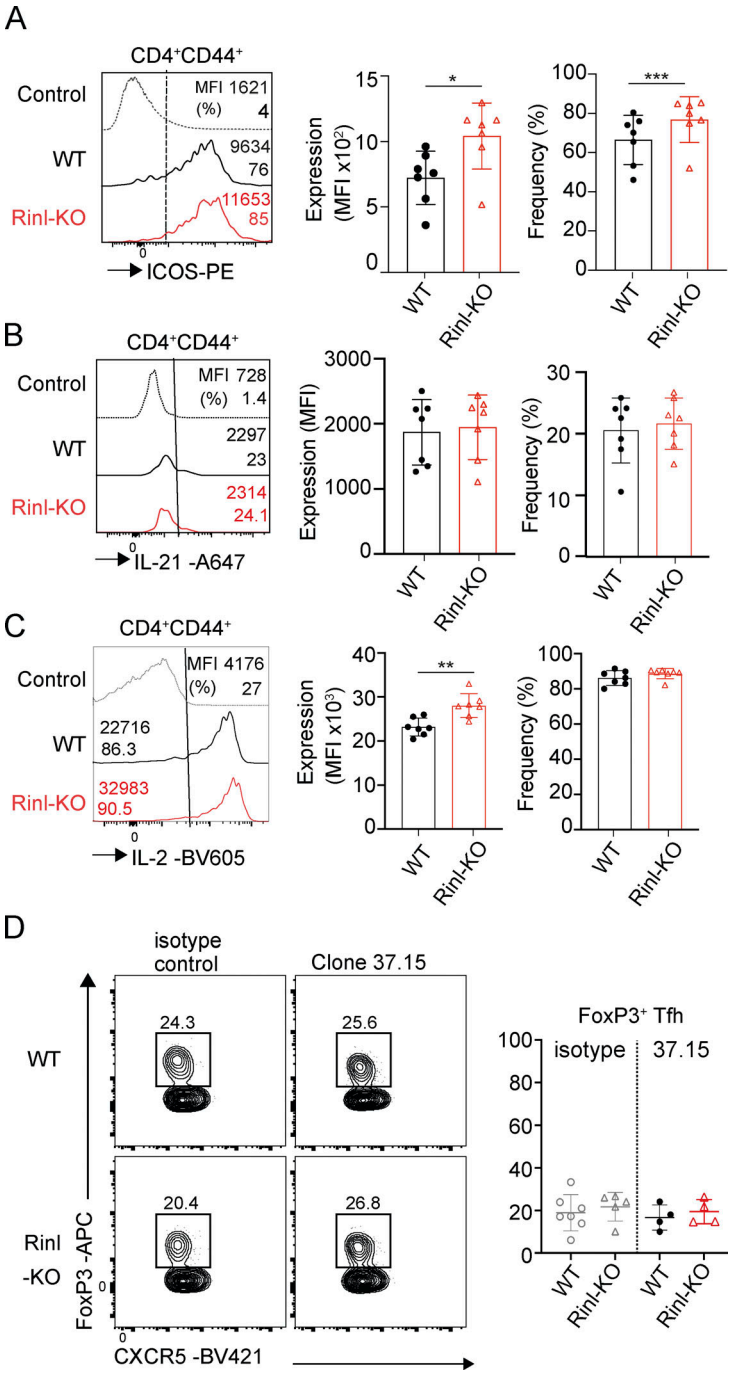

Figure S5. **Rinl controls ICOS and IL-2 expression in effector CD4⁺ T cells. (A)** Representative histograms of ICOS expression in effector CD4⁺ T cells (CD44⁺). A summary of ICOS expression (left diagram) and frequencies of ICOS⁺ cells among effector CD4⁺ T cells (right diagram) is shown alongside. **(B)** Representative histograms of IL-21 production in effector CD4⁺ T cells (CD44⁺). A summary of IL-21 expression (left diagram) and frequencies of IL-21⁺ cells among effector CD4⁺ T cells (right diagram) is shown alongside. **(C)** Representative histograms of IL-2 production in effector CD4⁺ T cells (CD44⁺). A summary of IL-2 expression (left diagram) and frequencies of IL-2⁺ cells among effector CD4⁺ T cells (right diagram) is shown below. **(D)** Representative contour plots of follicular Treg cells (Tfr) of WT and Rinl-KO mice treated with isotype control or αCD28 (Clone 37.15) 1 d before immunization. Analysis is shown alongside. Summary of 7–8 (A–C) and 4–7 (D) mice that were analyzed in two independent experiments are shown. Mean ± SEM are shown along individual data points in the graphs. Data were statistically analyzed using unpaired two-tailed *t* tests. *P < 0.05, **P < 0.01, ***P < 0.001.